Lawrence Berkeley National Laboratory
Recent Work

## Title

CHARACTERISTICS OF FRAGMENTS PRODUCED IN THE INTERACTION OF 5.5-GeV PROTONS WITH SILVER

## Permalink

https://escholarship.org/uc/item/0161j659

## Authors

Hyde, Earl K.
Butler, Gilbert W.
Poskanzer, A.M.

## Publication Date

1971-05-01

eScholarship.org Powered by the California Digital Library
University of California

Submitted to Physical Review

UCRL-19991
Preprint

RECEIVED
LAWRENCE
RADIATION LABORATORY

DOCUMENTS SECTION

# CHARACTERISTICS OF FRAGMENTS PRODUCED IN THE INTERACTION OF 5.5-GeV PROTONS WITH SILVER

Earl K. Hyde, Gilbert W. Butler, and A. M. Poskanzer

May 1971

AEC Contract No. W-7405-eng-48

TWO-WEEK LOAN COPY

*This is a Library Circulating Copy which may be borrowed for two weeks. For a personal retention copy, call Tech. Info. Division, Ext. 5545*

LAWRENCE RADIATION LABORATORY
UNIVERSITY of CALIFORNIA BERKELEY

UCRL-19991 c.2

## DISCLAIMER

This document was prepared as an account of work sponsored by the United States Government. While this document is believed to contain correct information, neither the United States Government nor any agency thereof, nor the Regents of the University of California, nor any of their employees, makes any warranty, express or implied, or assumes any legal responsibility for the accuracy, completeness, or usefulness of any information, apparatus, product, or process disclosed, or represents that its use would not infringe privately owned rights. Reference herein to any specific commercial product, process, or service by its trade name, trademark, manufacturer, or otherwise, does not necessarily constitute or imply its endorsement, recommendation, or favoring by the United States Government or any agency thereof, or the Regents of the University of California. The views and opinions of authors expressed herein do not necessarily state or reflect those of the United States Government or any agency thereof or the Regents of the University of California.

# CHARACTERISTICS OF FRAGMENTS PRODUCED IN THE INTERACTION OF 5.5-GeV PROTONS WITH SILVER*

Earl K. Hyde, Gilbert W. Butler†, and A. M. Poskanzer

Nuclear Chemistry Division
Lawrence Radiation Laboratory
University of California
Berkeley, California 94720

May 1971

## ABSTRACT

The energy spectra of nuclear fragments produced by the interaction of 5.5-GeV protons with silver were determined at several laboratory angles by means of dE/dx-E measurements with semiconductor detector telescopes. Individual isotopes of the elements from hydrogen to nitrogen were resolved. From oxygen to silicon the elements were determined without isotopic separation. For the case of the isotopes of He through Be enough of the evaporation-like energy spectra were recorded so that it was possible to perform integrations to obtain angular distributions and total cross sections. For elements above beryllium an experimental cutoff on the low-energy side precluded these integrations and only the high-energy portions of the spectra were recorded. The energy spectra of the neutron-deficient isotopes differ from the others in that the high-energy parts of the spectra are more pronounced and flatter, and the angular distributions are more forward peaked.

Some of the energy spectra were fitted with calculated curves based on the isotropic evaporation of fragments from an excited nucleus moving along the beam axis. The apparent Coulomb barriers obtained from this analysis were about one half the nominal Coulomb barriers and the apparent nuclear

temperatures fell in the 8-11 MeV range. However, no one temperature could fit the entire energy range and for the highest energy fragments observed at 90° the apparent temperature rose to 20 MeV or higher. From the forward-backward shifts of the most probable energy it was deduced that the average velocity of the moving system emitting Li and Be fragments is 0.008 c. However, all of the data are more forward peaked in intensity than can be explained by the simple two-step model. The energy analysis carried out on these new data is compared to those given in the literature for silver targets or emulsions bombarded with protons, cosmic rays, pions, kaons, and other particles. Comparisons are made of these results with those obtained in an earlier study of fragments from a uranium target.

# I. INTRODUCTION

In a recent study we described the application of silicon semiconductor detectors incorporated in a particle identifier system for the study of fragments resulting from the disintegration of uranium target nuclei bombarded with 5.5-GeV protons.[1] The present study describes the results of a similar investigation of the fragments produced by a silver target bombarded with 5.5-GeV protons. In a series of measurements with ΔE and E detectors of various thicknesses it was possible to identify individual isotopes of the elements hydrogen through nitrogen and to measure the energy spectra for the individual isotopes at 5 angles to the beam. The energy distributions have Maxwellian shapes resembling evaporation spectra but because of an instrumental low-energy cutoff it was not possible to observe the maxima of the Maxwellian distributions for fragments heavier than beryllium. For fragments heavier than nitrogen it was not possible to obtain isotopic identification with the telescope containing the thinnest ΔE detector but individual elements up to silicon were resolved and the high-energy segments of the energy spectra were measured.

Silver was chosen as the target in order to obtain data to compare with the fragment characteristics reported in many previous studies done by other methods. The nuclear emulsion technique has been most widely used because of the ease of study of the interaction of high-energy particles with AgBr in the emulsion. In most studies the emulsion was used both as target and detector. The bombarding particles have been cosmic rays,[2-11] machine accelerated protons of 0.5 to 30 GeV,[12-39] π-mesons,[5,40-45] antiprotons,[36,46-50] K-mesons,[51-53] and other projectiles. In some cases the emulsion has been used to detect fragments produced in an external target of metallic silver.[14-16]

Fragments from silver have also been studied by techniques based on mass spectrometry[54] or on the measurement of the radioactivity of the fragments.[55-62]

Each experimental method has certain advantages and shortcomings. Methods based on fragment radioactivity are limited in scope because they can be applied only to a small fraction of the products, but they do have great sensitivity and specificity. They have been particularly valuable for exploring yield variations over many orders of magnitude as the energy of the bombarding particle is changed. In general, these techniques supply only yield data but some studies have been done in a way to extract information on fragment energy spectra and angular distributions. However, radioactivity-based methods provide no information concerning the other particles emitted in the nuclear interactions leading to the production of the isolated radioactive product. The nuclear emulsion technique has some strong disadvantages because of the labor involved in getting statistical accuracy on individual fragments, the difficulty of making a clean identification of the charge and mass of individual fragments from the characteristics of the tracks, and from uncertainty in the target nucleus. Because of the identification problem the great bulk of the published work has been done on $^{8}Li$, $^{8}Be$ and $^{9}B$, which decay in such a way that an easily identified hammer track is produced. To be set against these disadvantages is the fact that the nuclear emulsion technique makes it possible to examine all the charged particles (mostly, protons and helium ions) coming from an individual nuclear disintegration (star) and to study the correlation of these other particles with the fragment. For example, it is possible to study the yield and energy spectrum of the identified fragment as a function of the number of gray, black, and sparse prongs in the star.

Such correlations provide a much deeper understanding of the underlying reaction mechanism. The nuclear emulsion technique also provides the opportunity to study cases in which more than one fragment is emitted in a single disintegration. In the semiconductor technique as applied by ourselves, or by others,[63,64] it has been possible to measure energy spectra with good statistics for a number of fragments each precisely identified by atomic number and mass number. All stable and radioactive species are measured--the only requirement is that the fragment be stable toward heavy particle emission. The method has the limitation of a low-energy cutoff that increases as the fragment charge increases. Furthermore, as applied in the study reported here, no additional information is obtained on the characteristics of other particles produced in the nuclear break-up giving rise to the observed fragment.

Because conclusions from previous studies have been stated many times in the references already cited and in several review articles[65-67] it is not necessary to present them in detail here, but it may be of some use to set down a short summary of the main deductions, particularly those which have relevance to the later discussion of our own data. In the following text the word fragments refers to nuclei of charge 3 or higher. The usual nuclear emulsion terminology on track types will be followed: gray tracks are considered to be caused by cascade protons, black tracks are attributed to evaporated protons or helium ions, and sparse tracks are assigned to $\pi$-mesons or other particles of minimum ionization. The conclusions of previous studies are:

1) Fragment yield increases strongly with the energy of the bombarding protons from 100 MeV to about 2 GeV and then remains relatively constant up to 30 GeV. We have summarized in Table I the bulk of the published data on

fragment yields for proton bombarding energies in the GeV range.

2) For proton bombarding energies of 1 GeV or greater the yield variation for fragments close to beta stability such as $^{18}F$ and $^{24}Na$ varies in an interesting way with the atomic mass of the target.[59] For the lighter target elements up to about mass 100 the yield decreases with an increase in target mass, whereas for the heavier targets the trend reverses and there is an increase in fragment yield as the target mass increases. This has been interpreted as evidence for a change in the reaction mechanism leading to fragment formation. This feature is interesting for the case of silver because silver is near the minimum of the fragment yield versus target mass curve.

3) Fragment yield increases with the complexity of the nuclear star: i.e., with the number of gray, black, and sparse prongs.

4) The greatest yields occur for products near beta stability.[65,67] This fact reduces the significance of conclusions drawn from a study of radioactive fragments alone.

5) In those cases in which the short black track of the residual nucleus can be identified it is strongly correlated in direction with the direction of the fragment track, the angle 180° being favored.[12,35,65,68]

6) The fragment energy spectra have shapes resembling, at least roughly, the Maxwellian distribution expected for an evaporation process. Since this is such an important feature we comment more fully on it.

Many authors have made the attempt to fit curves based on evaporation theory to their energy data. Some representative papers may be singled out[6,22,35] for a discussion of this fitting. One common practice is to compare the data taken at all angles to the following simple formula taken

from LeCouteur's treatment of the Weisskopf evaporation theory.[69]

$$P(\epsilon)d\epsilon = \frac{\epsilon - B}{\tau^2} \exp\left(-\frac{\epsilon - B}{\tau}\right) d\epsilon \qquad (1)$$

Here $P(\epsilon)d\epsilon$ is the probability of emission of a fragment with disintegration energy $\epsilon$ in the interval $d\epsilon$ from a nucleus excited to a temperature $\tau$ and characterized by a barrier B to the escape of the fragment. To correct for recoil during the escape of the fragment the disintegration energy $\epsilon$ is related to the observed energy E by the equation, $E = (1 - m/M)\epsilon$, where m and M refer to the mass of the fragment and the emitting nucleus, respectively. This correction has often been ignored, but it is important. If the experimental data are sufficiently extensive to define the energy spectrum at several angles it is possible to employ revised equations (see References 6, 22, 34, 35, and 70, for example) which allow for the effect on the spectrum of the velocity, v, of the excited nucleus that emits the fragment.

In Table II we summarize the $\tau$, B, and v parameters reported by representative authors to describe fragment spectra from proton bombarded emulsions. Most of these are for $^{8}$Li hammer tracks but there are some for Li, Be, B, C, and N identified by the track area method. A particularly complete set of data has been published by Stein[35,39] for the case of 25-GeV proton bombardment. Additional data for emulsions bombarded with other types of particles are collected in Table III.

In these tables the temperature parameter falls in the range of 10-15 MeV which is regarded by many authors as a physically unreal value because if all nucleons in the nucleus were in fact raised to this energy the total nuclear excitation energy would exceed the total binding energy of the

nucleus. The Coulomb barrier parameter B is universally found to be lower than would be estimated for the emission of the fragment from a silver nucleus, even when allowance is made for the reduction in nuclear charge of the parent nucleus by the loss of charged particles in the cascade step. Ideas which have been advanced to account for this barrier lowering include the increase of the nuclear radius by nuclear expansion at high temperature,[71] the occurrence of large amplitude surface vibrations,[72] and the formation of highly deformed nuclei.[73,1]

The moving system velocity parameter, v, falls in a range which seems reasonable although the value deduced from the analysis is somewhat higher than that expected on the basis of estimates from Monte Carlo calculations of the cascade step. There should also be a correspondence between this parameter and the forward-to-backward ratio for fragment emission. Most authors are successful in reconciling the two values obtained from the analysis of their data but a few report an inconsistency in this regard. This inconsistency is always in the direction of more forward peaking than expected.

While it is true that this empirical curve fitting is successful for the main part of the energy spectrum, it is almost uniformly reported that it is not successful for the highest fragment emergies, particularly at forward angles. The excess of fragments at the higher energies may represent contributions from the cascade step but direct knock-out of nuclear clusters by the incident particle is discounted[8-12] as the mechanism of this contribution. Various hypotheses concerning the possible role of nuclear interactions by the cascade particles with nucleonic clusters in the nuclear surface have been formulated but no formal theory has been proposed for fragments heavier than helium ions.

It is an interesting fact also that the fragment energy spectra do not vary much with proton bombarding energy. Perfilov, Lozhkin, and Shamov[65] in their review of this point state that no appreciable change occurs in the proton energy range 660 MeV to 6.2 GeV. This is apparent also from the entries in Table II. There are greater changes when mesons or antiprotons are substituted for protons (see Table III) but these changes are not as great as one might have expected. Stein[36] reports that the fragment energy spectra in nuclear emulsions bombarded with 5-GeV antiprotons and with 25-GeV protons are quite similar.

In Sec. IV at the end of this paper we present the results of a similar curve fitting to our own data, including comments on the agreement or disagreement with the values listed in Table II and on our interpretation of the meaning of the parameters. In Sec. II we describe our experimental methods and in Sec. III we present the results.

## II. EXPERIMENTAL

Thin targets of silver were placed in a 36-in. diameter target chamber located in one of the 5.5-GeV external proton beams of the Bevatron. Fragments ejected from the target were measured in a telescope of silicon semiconductor detectors. The electronic system associated with these detectors is shown in Fig. 1. It identified each fragment and produced output signals characteristic of the particle type and its energy. These signals were fed to an analog-to-digital converter and then to a small computer which produced histograms of the particle spectra and of the energy spectra of individual fragments. Complete details of the electronic circuitry and identification techniques are given in Ref. 1.

Self-supporting silver metal targets with thicknesses of 1.02, 7.14, and 25.9 mg/cm$^2$ were used. All the foils were larger than the beam size, which was typically 1/2 in. wide by 3/8 in. high. In addition 1-mg/cm$^2$ target was mounted on a frame made of 0.0-025-in. Mylar. Beam pulses 0.8 sec long and containing about $3 \times 10^{11}$ protons occurred every six seconds.

The fragment telescope consisted of three phosphorus-diffused or lithium-drifted silicon detectors with associated collimators mounted on an arm which could be positioned at any angle to the beam from 20° to 160°. Table IV is a listing of the detector telescopes used in this work. The reason for the variety was that it was not possible to measure the entire energy spectrum with one counter telescope nor was it possible to achieve good particle identification for all fragments by use of a single choice of thicknesses for the ΔE and E detectors. It was necessary to combine data from experiments made with two or more different combinations of detectors in order

to determine the energy spectra over a broad energy range. A monitor telescope provided the necessary information for a normalization of the data from different experiments, as described in Ref. 1. The data were corrected for the fraction of events rejected by the pile-up rejector and the fraction lost because of computer dead time. The energy spectra were corrected also for absorption in the target and the dead layers of the counters.

Representative particle spectra from this experiment are shown in Fig. 2. Most of the spectra in Fig. 2 were obtained with a telescope containing a 61-μm ΔE detector. The particle spectra for the telescopes utilizing a 20-μm ΔE detector were not as good as those in Fig. 2, but they allowed us to extend the measurements to lower energies for the isotopes of H, He, Li, Be, and B. Parts of the energy spectra always overlapped and in some cases where there was a discrepancy the 20-μm data were normalized to the data of the thicker telescope. Also, in the case of telescopes using a 3-mm or a 5-mm E counter, pile-up effects distorted the particle spectra and these results were normalized where they overlapped with data from thinner telescopes. Figure 3 shows a particle spectrum from a telescope with a 20-μm ΔE detector in which element resolution was achieved but individual isotopes were not separated.

Examples of semi-logarithmic plots of data taken with three detector telescopes for the nuclides $^{4}He$, $^{6}Li$, and $^{7}Be$ are shown in Fig. 4.

## III. RESULTS

The laboratory energy spectra determined in this study are shown in Figs. 5 through 11. For isotopes of H, He, Li and Be it was possible to measure enough of the spectrum to establish that all had the general appearance of a Maxwellian evaporation spectrum similar to that known from previous work on $^{8}$Li. For these isotopes it was possible to extrapolate yields to zero energy and to integrate the curves at each of the 5 angles studied in order to derive the angular distributions. These distributions were integrated in turn to obtain relative total formation cross sections. These relative cross sections were normalized to obtain the absolute values listed in Table V by assigning 17.4 ± 0.8 mb to the $^{7}$Be production cross section. This absolute value was determined radiochemically, as described in the appendix of Ref. 1.

For the hydrogen isotopes it was possible to observe the maxima of the curves at all angles although the data do not determine with precision the shift of this maximum with change in angle. Also, the hydrogen isotope spectra extend out only to 30-40 MeV because at higher energies these particles penetrated the thickest detector telescopes used.

In the case of helium and lithium good data were obtained on the prominent isotopes $^{3}$He, $^{4}$He, $^{6}$Li, and $^{7}$Li. The curves for the less prominent isotopes $^{6}$He, $^{8}$Li, and $^{9}$Li were more poorly defined particularly as to the exact location of the most probable energy.

The data on $^{9}$Be and $^{10}$Be extend down just below the maxima of the spectra, which made it possible to estimate the missing sections down to zero energy. The $^{9}$Be and $^{10}$Be data were of comparable quality at all angles but

the $^{7}$Be data at 20° and 160° were less definite in the peak region because of some background effects in those particular runs.

At boron the experimental low-energy cutoff is near or slightly above the maximum in the energy spectrum so that we can only specify an upper limit for the most probable energy. For elements above boron only a section of the energy spectrum lying well above the turnover point could be studied. Hence, it was not possible to extrapolate the curves to zero energy and to make the integrations necessary to determine angular distributions and total yields. In this respect this study of fragments from silver was considerably restricted compared to our previous study of fragments from uranium[1] in which we were able to define the region of the energy maximum for all products up through isotopes of carbon. The reason for the difference is that, while the experimental cutoffs are the same in the two experiments, the fragments from silver leave behind much lighter residual nuclei and therefore have greatly reduced energy from Coulomb repulsion.

In the case of the Li and Be fragments from silver we call attention to the fact that the cross section increases at the more forward laboratory angles and that the positions of the maxima in the energy spectra move to slightly higher energies. This is the expected behavior for emission of fragments from an evaporating nucleus having a forward momentum component. This again is in agreement with the literature reports on $^{8}$Li hammer tracks.

It may also be remarked that the neutron-deficient isotopes have energy spectra with smaller slopes in the high-energy region than do heavier isotopes of the same elements. This is evident in Fig. 12 where all the curves at 90° to the beam are displayed on a single semilogarithmic plot. Here all the solid

curves show roughly the same slope at high energy but the broken curves which represent the neuton-deficient isotopes of $^{3}He$, $^{6}Li$, $^{7}Be$, $^{8}B$, $^{10}B$, $^{10}C$, and $^{11}C$ are distinctly flatter. Such a difference could be explained by the supposition that neutron-deficient fragments are produced from nuclei which are excited to a higher nuclear temperature as a result of events with larger deposition energy in the fast nucleonic cascade.

In Fig. 13 are displayed the segments of the energy spectra measured for the elements carbon through silicon at three angles to the beam. The differential cross sections of the elements decrease with increase in atomic number, which is qualitatively different from the analogous data[1] for an uranium target.

In Fig. 14 are shown the laboratory angular distributions obtained by integrating those energy spectra which could be extrapolated to zero energy. All the angular distributions are similar except those for the hydrogen isotopes, for which the data do not extend into the high energy region. For $^{3}He$, $^{9}Be$ and $^{10}Be$ small corrections were made for the extrapolation to high energies. From these angular distributions the fraction of the events in the forward and backward hemispheres were determined and the ratio was entered in Table V. The values for $^{3}He$ and $^{4}He$ are somewhat less than those for the other nuclides. The heavier isotopes of Li are somewhat more prominent in the forward direction than are the lighter isotopes although in this connection the values for $^{8}Li$ and especially $^{9}Li$ are much less well determined than those of the more abundant $^{6}Li$ and $^{7}Li$. Our F/B value for $^{8}Li$ agrees with the literature values quoted in Tables II and III for proton or cosmic ray induced stars.

The angular distributions were integrated in order to obtain the total production cross sections shown in Table V. Some comments can be made about our cross section values. Our value of 12.8 mb for $^{8}$Li is considerably larger than the literature values quoted in Table I, which fall in the 3 to 6 mb range for 2-GeV proton bombardments and 5 to 8 mb for 6-9 GeV proton bombardment. Our value of 17.4 mb for $^{7}$Be determined by a radiochemical method is close to the value of 18.2 mb determined by Hudis and Tanaka for 3-GeV protons on silver. The sum of our cross section values for $^{7}$Be, $^{9}$Be and $^{10}$Be is 43 mb, which is in rough agreement with the value of 30 mb reported by Gorichev, Lozhkin, and Perfilov for total Be (exclusive of $^{8}$Be) in the interaction of 6-GeV protons with AgBr in emulsions.

If we compare our cross sections with those determined in our earlier study of uranium[1] we note that our total He, Li, and Be yields are lower and are decreasing faster with increasing Z in the case of the silver target. This is also evident in the element yields up to Si, as has already been pointed out. Also, both from the cross section data and from an examination of the particle spectra in those cases where total yields were not obtained, it is clear that the yield distribution for isotopes of each element are narrower for the silver target case and that the peak of the yield distribution is very evidently 1/2 to 1 mass unit less neutron excess than in the case of uranium.

## IV. DISCUSSION

### A. Empirical Fitting to an Evaporation Expression

It is useful at this point to attempt a fit of our energy spectra to an evaporation expression in order to determine how well the spectra can be described in this manner and to extract parameters which can be compared to those given in the literature for $^{8}$Li and a few other nuclides. In comparison to the previous studies we have the advantage of better statistics over a broader range of fragment energies, a clear identification of many more species than only $^{8}$Li, and a separation of the data into spectra at 5 angles with respect to the beam. On the other hand some of the important parameters, such as the center-of-mass velocity, are crucially dependent on the shape of the spectra in the region of the maxima near the effective Coulomb barrier and it is here that our data are least certain in several instances owing to the instrumental cutoff at low energy.

We represented the energy spectrum in the moving system of the evaporating nucleus by the expression

$$P(\epsilon) = \sum_{k=\langle k\rangle - \Delta}^{\langle k\rangle + \Delta} (\epsilon - kB)e^{-(\epsilon - kB)/\tau} \quad , \epsilon > kB \quad , \qquad (2)$$

where $\epsilon$ is the disintegration energy, B is the nominal Coulomb barrier and kB is the effective Coulomb barrier. Summation of several distributions calculated for values of k ranging from below and above an average value $\langle k\rangle$ by an amount $\Delta$ was included in order to reproduce the widths of the experimental spectra. This factor $\Delta$ is not the uncertainty in k but the amount

of smearing of $k$ needed to reproduce the width of the peaks. Except for this smearing the expression (2) is identical with Eq. (1) given earlier. The factor $\tau^2$ has been removed from the denominator as it does not affect the shape of the spectra and we were interested only in the shapes.

The nominal Coulomb barrier $B$ was computed by a tangent spheres estimate from the Z and A values of the fragment and the residual nucleus by use of a radius parameter of 1.44 Fermis. We estimated that $_{43}Tc^{96}$ was a reasonable choice for the average emitting nucleus from a consideration of past discussions[74,76] of the knock-on cascade step in the interaction of GeV protons with a complex nucleus like silver. The results are rather insensitive to this choice as verified by substituting $_{45}Rh^{100}$ or $_{40}Zr^{92}$ for the emitting nucleus in test calculations.

The energies of fragments of mass A were corrected for the recoil of the residual nucleus and related to a velocity V, in the moving system by the equation

$$\frac{96-A}{96} \in = \frac{1}{2} mV^2 \quad . \tag{3}$$

At 90° the laboratory energy, E, was taken equal to $\in (96-A)/96$. To calculate $V_L$, the laboratory velocity, for the 20° and 160° spectra, the velocity of the moving system, v, was simply added to and subtracted from V, respectively. This is strictly true at 0° and 180°, respectively, and is in error by $0.06(v/V)$ at our angles, which distorts the calculated spectra, but mainly below our low-energy cutoff.

The laboratory cross sections were calculated from $P(\in)$ via the relationship:

$$\frac{d^2\sigma}{dEd\Omega} = P(\in) \frac{E}{\in} \frac{d\in}{dE} \quad . \tag{4}$$

This is proportional to $P(\in)\sqrt{E/\in}$ / $(dV_L/dV)$. The quantity $dV_L/dV$ would be equal to 1 in the absence of a correlation between V and v. We used a correlation of the form

$$\frac{v - \langle v \rangle}{\langle v \rangle} = n \frac{V - \langle V \rangle}{\langle V \rangle} \quad , \tag{5}$$

where the average quantity $\langle V \rangle$ was taken to be the root-mean-square V obtained from the average energy $\langle \in \rangle$, which is equal to $\langle k \rangle$ B + 2τ for a Maxwellian distribution. A positive correlation factor n means that fragments emerging from the moving system with more than average velocity are emitted from parent nuclei having a greater than average moving-system velocity.

In the first stage of the analysis families of computer calculated curves were compared with the 90° spectra to determine "best" values of the parameters τ, $\langle k \rangle$ , and Δ. It was found that more than one value of τ was necessary. This fact in itself makes it questionable whether it is possible to extract meaningful parameters with this simple functional form. Perhaps the fact that 90% or so of the cross section falls in the peak region where a single temperature value applies is justification for proceeding. The temperature values listed in Table VI gave a reasonably good fit around the maximum in the spectrum but there was a continuous change to higher temperatures above the maximum. In Table VI the temperature parameter, $\tau_{HE}$, gives the temperature which fits best at the highest portion of the spectrum recorded at 90°.

Our values of $\tau$ for the lithium isotopes are considerably lower than the literature values for $^{8}$Li given in Table II. As far as the effective Coulomb barrier is concerned we agree with the literature in finding that the values required to fit the data are substantially lower than the nominal Coulomb barriers obtained from tangent spheres. The $\langle k \rangle$ values of 0.4 to 0.55 listed in Table VI agree with the values we obtained in the study of fragments from uranium and our discussion in that paper[1] of the possible reasons for this striking phenomenon can apply as well to the present results. Other authors who comment on possible explanations of this phenomenon are cited in the Introduction. However, our $\langle k \rangle$ B values are somewhat larger than the effective barrier values listed in Table II. This may be related to the fact that our values were determined from 90° data whereas most of the literature values came from an analysis of data at all angles. Also in some of the studies in the literature no correction was made for the recoil sharing of the disintegration energy between fragment and its residue; if the data points are not corrected for this the fitted value of the effective barrier is lowered.

The experimental data at 20° and 160° were used to determine a value for the velocity of the emitting system. We computed sets of curves for various values of v and n and compared them to the data. The selection of the v value was made on the basis of the shift of the position of the most probable energy from 20° to 160° and is dependent on the quality of the data in the peak portion of the spectrum. The results are entered in Table VI. The $^{3}$He and $^{4}$He spectra showed no shifts in the location of the peak from 20° to 160°. This corresponds to a low average velocity for the emitting nucleus and is in keeping with the ease of emission of such fragments from nuclei at all levels of excitation down to the lowest.

The values for $^{6}$Li and $^{7}$Li are rather well determined within the limits stated while the data for $^{8}$Li, $^{9}$Li, and $^{7}$Be provide only a rough indication of v. For $^{7}$Be it is clear that the velocity is greater than the 0.006 c value measured for the heavier isotopes but the 20° data in this case were not clear cut and a better value was not established. However, we have a real discrepancy with the values listed in Table II. Our values are substantially lower than the literature values except that we do have agreement with several of Stein's values.[35]

Attempts to determine values of the correlation parameter, n, defined by Eq. (5) were only partially successful. In the case of the $^{3}$He and $^{4}$He spectra it became clear that no combination of $\tau$, v, and n could explain the increase in the high-energy parts of the spectra in going from 160° to 20°. The difficulty stems from the fact (seen clearly in Fig. 6) that the increase in the spectra between 160° and 90° is much less than that between 90° and 20°, i.e. there is a much stronger probability of forward ejection of energetic $^{3}$He and $^{4}$He than can be explained by any simple evaporation model. The 45° and 20° data may have a big contribution from the knock-on cascade step of the reaction[74] or from the pre-equilibration evaporation step.[75] The analysis of the $^{6}$Li and $^{7}$Li data definitely indicated a need for an n value of 2 ± 0.5, but even with this strong correlation the data in the high-energy parts of the spectra indicated a favoring of emission in the forward direction. The quality of the fit to the $^{7}$Li data can be seen in Fig. 15. The beryllium data also indicated the need for a positive correlation of v and V and a somewhat better description of the 20°-90°-160° data could be obtained from the calculated curves, as shown in Fig. 16.

For the element spectra for carbon through silicon some correction of v and V is seen to be required just by an inspection of Fig. 13. There is a change in slope between 20° and 160° whereas with no correlation of v and V the slopes at high energy should be the same. If we assume a moving system velocity of 0.006 v/c the value of n which gives agreement with the data is about 1. Carbon, which can be taken as typical of the group is shown in Fig. 17. Over the limited range of experimental data the element spectra from carbon to silicon can be described by the evaporation model much better than the Li, Be, and B spectra. However, it cannot be determined from our data how good the fit is in the crucial peak region of the spectra.

## B. Comparison with Stein's Results

One of the most extensive previous studies of fragments from silver is the emulsion study carried out by Stein[35-39] for 25-GeV protons. It is to be expected that there will be differences in the results between 5.5-GeV and 25-GeV proton energy but it is interesting nonetheless to compare the fragment characteristics found in the two studies. See Table VII.

For the lithium isotopes the agreement is reasonably good if we compare values for $E_p$, $\tau$, V or $\langle k \rangle$ B, center-of-mass velocity, and F/B ratio. The main difference is the higher effective Coulomb barrier and F/B ratios found in the present study. Also Stein finds a slight shift to higher energy, which we do not see, for the most probable energy of $^{6}$Li and $^{7}$Li compared to $^{8}$Li, but this is not a large disagreement.

In the beryllium isotopes there are larger differences. Stein reports most probable energies for $^{7}$Be and $^{9}$Be of 37 and 43 MeV, respectively, whereas we report 22 to 20 MeV, respectively. On the other hand Stein's value of 23 MeV for $^{8}$Be is in excellent agreement with our values for $^{7}$Be and $^{9}$Be. There is a similar discrepancy in the boron data. We do not observe the turnover point in the spectrum but we can place the most probable energy, $E_p$ at < 26 MeV for $^{8}$B and $^{10}$B whereas Stein reports a turnover at $\sim$40 MeV and at 47 MeV, respectively, for these isotopes. Also in our spectra for the unseparated isotopes of carbon and nitrogen we see no turnover down to carbon energies of 33 MeV and nitrogen energies of 38 MeV whereas Stein reports a turnover for $^{12}$C at 45 MeV and one for $^{14}$N at 65 MeV.

The trend of these results indicates that in those cases where the emulsion tracks give a unique identification of the fragment (e.g. $^{8}$Li and $^{8}$B identified by a hammer track), there is fairly good agreement between the two studies. On the other hand, for Be and higher Z elements, where the emulsion identification must be made by the track-area method, there are discrepancies which are in the direction to indicate that there is a considerable loss of events at the lower part of the spectrum. We have no experience with emulsion techniques so we cannot make a personal evaluation of the problem but we note that several authors have discussed[5,6,40] the great difficulties in using the track-area method at the lower end of the energy scale. Stein was well aware of these difficulties and discussed them at length in his thesis, but was satisfied that his improvements in technique had pushed the method down to the energy ranges which he quoted in his final results. The discrepancies we have found here suggest there may be some remaining difficulties. However, we must

repeat that our results are for 5.5-GeV protons while Stein's are for a 25-GeV energy and there could be real differences in the fragment characteristics.

### C. Application of Two-Step Model of High-Energy Reactions

The evaporation analysis discussed in the Introduction and applied by us in Sec. IVA is well known to be grossly oversimplified because a variety of nuclei of different charge, mass, and excitation are produced in the initial encounter of the target nucleus with GeV particles.[74] One can still justify the analysis partly on the grounds that fragment emission is strongly dependent on nuclear excitation so that the observed fragment energy spectra are representative chiefly of the fragments formed only from the most highly excited nuclei remaining after the fast cascade step. Nonetheless, a more proper way to compute the expected contribution of evaporation processes to the observed fragments is to start with the set of excited nuclei computed from a Monte Carlo calculation of the cascade step and to apply evaporation theory to each nucleus in this set. Since the usual excitation is very high, several particles and/or fragments must be emitted before the nucleus is de-excited and thus a Monte Carlo technique is again an appropriate mathematical method for this complex problem. This approach to the prediction of the properties of nuclear evaporation in high-energy reactions is discussed elsewhere[76,77] where the problems, limitations, and successes are outlined. Katcoff, Baker, and Porile[16] carried through such an analysis to describe the properties of $^{8}$Li fragments ejected from Ag targets bombarded with 2-GeV protons. Their calculation predicts that the peak in the energy spectrum should occur near 20 MeV for $^{8}$Li emitted at 90° to the beam and that this peak energy should shift slightly higher and lower

for fragments emitted at forward and backward angles. This result is in reasonable agreement with the experimental data obtained by those authors and with the Li data obtained in the present study.

On the other hand, these authors found that the shape of the calculated and experimental spectra agreed only roughly. The experimental spectra were broader and had more intensity in the low-energy part of the spectrum as well as in the high-energy portion well above the maximum. Furthermore, the experimental angular distributions were more forward peaked than predicted by the calculation.

Grigor'ev and co-authors[15] did a similar detailed calculation of the predictions of the cascade-evaporation model for the case of $^{8}$Li produced by nuclear evaporation during the interaction of Ag targets with 660-MeV protons. The results of this calculation were compared with experimental data taken by the authors. In order to get agreement between theory and experiment it was necessary to use an effective Coulomb barrier which was 0.7 the nominal barrier. These authors found gross discrepancies between theory and experiment on the shape of the spectra and angular distributions and concluded that it was impossible to describe all the data on the basis of a statistical decay of excited nuclei.

The conclusions of both these papers are in agreement with the discussion in Sec. IVA of our attempts to fit our data with a very general evaporation spectrum. We also see an excess of events in the high-energy region of the spectrum. We also are unable to select a set of evaporation parameters including a center-of-mass motion parameter which will generate a satisfactory simultaneous representation of the energy spectra at 20°, 90°, and 160°; the discrepancy is

in the direction to indicate a significant favoring of emission in the forward direction, as shown for example in Figs. 15 and 16.

## ACKNOWLEDGMENTS

We are indebted to R. Lothrop, M. Roach, and H. Sommer for the semiconductor detectors used in this work, to Donald Landis for advice and counsel on the electronic circuitry and to John Meng for his contributions in design and service to the on-line computer systems. We owe thanks to the Bevatron staff, not only for hospitality and the provision of the required beam, but for their considerable assistance in the installation of our apparatus in the external beam line.

## FOOTNOTES AND REFERENCES

*Work performed under the auspices of the U. S. Atomic Energy Commission.

†Present address: Chemistry Division, Argonne National Laboratory, Argonne, Illinois.

1. A. M. Poskanzer, G. W. Butler, and E. K. Hyde, Phys. Rev. C 3, 1 (1971).
2. S. O. C. Sörensen, Phil. Mag. 42, 188 (1951); 41, 946 (1949).
3. P. E. Hodgson, Phil. Mag. 42, 207 (1951).
4. D. H. Perkins, Proc. Roy. Soc. (London) A203, 399 (1950).
5. A. Alumkal, A. G. Barkow, G. Kane, R. E. McDaniel, and Z. O'Friel, Nuovo Cimento 17 (10), 316 (1960).
6. O. Skjeggestad and S. O. C. Sörensen, Phys. Rev. 113, 1115 (1959).
7. O. Skjeggestad, Arch. Math. Nature B57 (1959).
8. S. O. C. Sörensen, Phil. Mag. 42, 188, 325 (1951).
9. B. A. Munir, Phil. Mag. 1, 355 (1957).
10. S. J. Goldsack, W. O. Lock, B. A. Munir, Phil. Mag. 2, 149, 194 (1957).
11. S. Nakagawa, E. Tamai, and S. Nomoto, Nuovo Cimento 9 (10), 780 (1958).
12. O. V. Lozhkin and N. A. Perfilov, Sov. Phys. JETP 4, 790 (1957).
13. E. Baker and S. Katcoff, Phys. Rev. 123, 641 (1961).
14. S. Katcoff, Phys. Rev. 114, 905 (1959).
15. E. L. Grigor'ev, O. V. Lozhkin, V. M. Mal'tsev, and Yu. P. Yakovlev, Yad. Fiz. 6, 696 (1967); Sov. J. Nucl. Phys. 6, 507 (1968).
16. S. Katcoff, E. W. Baker, and N. T. Porile, Phys. Rev. 140, B1549 (1965).
17. M. Bogdanski, E. Jeannet, and C. Metger, Helv. Phys. Acta. 42, 485 (1969).
18. V. V. Avdeichikov, V. I. Bogatin, N. A. Perfilov, O. V. Lozhkin, and Yu. P. Yakovlev, Bull. Acad. Sci. USSR, Phys. Ser. 28, 1471 (1964).

19. S. Nakagawa, E. Tamai, H. Hurita, and K. Okudaira, J. Phys. Soc. Japan 12, 747 (1957).

20. O. V. Lozhkin, N. A. Perfilov, A. Rimskii-Korsakov, and J. Fremlin, Sov. Phys. JETP 11, 1001 (1960).

21. P. A. Gorichev, O. V. Lozhkin, and N. A. Perfilov, Sov. J. Nucl. Phys. 5, 19 (1967).

22. W. Gajewski, J. Pniewski, J. Sieminska, J. Suchorzewska, and P. Zielinski, Nucl. Phys. 58, 17 (1964).

23. O. V. Lozhkin, Zh. Eksp. Teor. Fiz. 79, 838 (1950).

24. S. Katcoff, Phys. Rev. 164, 1367 (1967).

25. M. Bogdanski, E. Jeannet, and C. Metzger, Helv. Phys. Acta. 42, 485 (1969).

26. N. A. Perfilov, N. C. Ivanova, O. V. Lozhkin, M. M. Markarov, V. I. Ostroymov, Z. I. Solov'ev, and V. P. Shamov, Zh. Eksp. Teor. Fiz. 38, 345 (1969).

27. N. P. Bogachev, E. L. Grigoriev, Yu. P. Merekov, and N. A. Mitin, Zh. Eksp. Teor. Fiz. 44, 493 (1963); Sov. Phys. JETP 17, 337 (1963).

28. W. Gajewski, J. Pniewski, T. Pniewski, J. Sieminska, M. Soltan, K. Soltynski, and J. Suchorzewska, Nucl. Phys. 37, 226 (1962).

29. W. Gajewski, T. Pniewski, J. Sieminska, M. Soltan, K. Soltynski, J. Suchorzewska, and K. Falkowski, Nucl. Phys. 45, 27 (1963).

30. W. Ko-Ming, Li Heui-Hsin, C. Nai-Chien, and Ho Mao, Acta Physica Sinica 22, 127 (1966); Chinese J. Phys. 22, 105 (1966).

31. N. P. Bogachev, A. G. Volod'ko, E. L. Grigoryev, Yu. P. Merekov, Zh. Eksp. Teor. Fiz. 44, 1869 (1963); Sov. Phys. JETP 17, 1257 (1963).

32. G. Baumann, H. Braun, and P. Cüer, Compt. Rend. 254, 1966 (1962); Phys. Letters 8, 146 (1964).

33. G. Baumann, Ann. Physique 9, 471 (1964).

34. D. A. Chakkalakal and A. G. Barkow, Nuovo Cimento 41, A249 (1966).

35. R. Stein, Contribution à l'etude experimentale de l'emission de fragments (Z = 3, a Z = 8) dans les noyaux de Brome et d'Argent des emulsions ionographiques par des protons de 25 GeV, Thèse, Strassbourg 1965; Nucl. Phys. 87, 836 (1967).

36. R. Stein, J. Physique 27, 405 (1966).

37. R. Stein, J. Physique 27, 513 (1966).

38. R. Stein, Nuovo Cimento 44 (10), 896 (1966).

39. R. Stein, Nucl. Phys. 87, 854 (1967).

40. F. O. Breivik, T. Jacobsen, and S. O. C. Sörensen, Phys. Rev. 130, 1119 (1963); Nucl. Phys. 61, 321 (1965).

41. Yu. F. Gargarin and N. S. Ivanova, Zh. Eksp. Teor. Fiz. 45, 1763 (1963).

42. N. S. Ivanova, V. I. Ostroumov, and Yu. V. Pavlov, Sov. Phys. JETP 10 1137 (1960).

43. N. S. Ivanova, Sov. Phys. JETP 7, 955 (1958).

44. P. Cüer and D. M. Harmsen, Phys. Letters 9, 274 (1964).

45. E. Pickup and L. Voybogic, Can. J. Research 28A, 616 (1950).

46. G. Baumann, D. Henny, and P. Cüer, C. R. Acad. Sci. Paris 264, 1832 (1967).

47. G. Baumann, J.-P. Gerber, A. Bechdolff, J. Jousset, and M. Montret, C. R. Acad. Sci. Paris 266, 1046 (1968).

48. B. Indira, A. Shantalakshmi, A. A. Kamal, Proc. Phys. Soc. 89, 1061 (1966).

49. G. Baumann, J.-P. Gerber, A. Bechdolff, and P. Cüer, Nuovo Cimento 55A, 656 (1968).

50. S. Katcoff, Phys. Rev. 157, 1126 (1967).

51. G. Baumann, J.-P. Gerber, A. Bechdolff, H. Braun, P. Cüer, and D. M. Harmsen, Phys. Rev. 138, B350 (1965).

52. G. Baumann, J.-P. Gerber, A. Bechdolff, H. Braun, J.-P. Lonchamp, and P. Cüer, Nucl. Phys. 77, 557 (1965).

53. A. Bechdolff, et al., Nuovo Cimento 44A (10), 131 (1966).

54. J. Hudis, T. Kirsten, R. W. Stoenner, and O. A. Schaeffer, Phys. Rev. C 1, 2019 (1970).

55. I. Dostrovsky, Z. Fraenkel, and J. Hudis, Phys. Rev. 123, 1452 (1961).

56. S. Katcoff, H. R. Fickel, and A. Wyttenbach, Phys. Rev. 166, 1147 (1968).

57. J. Hudis and J. M. Miller, Phys. Rev. 112, 1322 (1958).

58. E. Baker, G. Friedlander, and J. Hudis, Phys. Rev. 112, 1319 (1958).

59. A. A. Caretto, J. Hudis, and G. Friedlander, Phys. Rev. 110, 1130 (1958).

60. J. Hudis and S. Tanaka, Phys. Rev. 171, 1297 (1968); J. Hudis, Phys. Rev. 171, 1301 (1968).

61. I. Dostrovsky, R. Davis, Jr., A. M. Poskanzer, and P. L. Reeder, Phys. Rev. 139, B1513 (1965).

62. F. S. Rowland and R. L. Wolfgang, Phys. Rev. 110, 175 (1958).

63. P. Boerseling, G. M. Raisbeck, and T. D. Thomas, unpublished study, 1969-1970.

64. R. D. Edge, C. W. Darden, W. F. Lankford, and H. D. Orr, III, Bull. Am. Phys. Soc. 13, 1445 (1968).

65. N. A. Perfilov, O. V. Lozhkin, and V. P. Shamov, Sov. Phys. Usp. 3, (60) 1 (1960).

66. N. A. Perfilov, O. V. Lozhkin, and V. I. Ostroumov, Yadernye Reakstii pod deistviem chastits vysokekh energii (Nuclear Reactions Induced by High Energy Particles), Acad. Sci. USSR, Moscow (1962).

67. M. Lefort, Ann. Phys. (Paris) 9, 249 (1964).

68. E. Makowska, J. Sieminska, M. Soltan, J. Suchorzewska, and S. J. St. Lorant, Nucl. Phys. 79, 449 (1966).

69. V. Weisskopf, Phys. Rev. 52, 295 (1937); K. J. LeCouteur, Proc. Phys. Soc. (London) A63, 259 (1950).

70. P. A. Gorichev and I. I. P. Yanov, Sov. J. Nucl. Phys. 2, 68 (1966).

71. T. Miyazima, K. Nakamura, and Y. Futami, Prog. Theor. Phys. Supplement 34, 621 (1965).

72. E. Bagge, Ann. Physik. 33, 389 (1938); Physik Zeit. 44, 461 (1942).

73. R. Da Silveira, Phys. Letters 9, 252 (1964).

74. N. Metropolis, R. Bivens, M. Storm, A. Turkevich, M. M. Miller, and G. Friedlander, Phys. Rev. 110, 185 (1958); 110, 204 (1958).

75. G. D. Harp, J. M. Miller, and B. J. Berne, Phys. Rev. 165, 1166 (1968).

76. I. Dostrovsky, Z. Fraenkel, and G. Friedlander, Phys. Rev. 116, 683 (1959).

77. J. Hudis, in Nuclear Chemistry, Vol. I, ed. by L. Yaffe, (Academic Press, New York, 1968), p. 169.

Table I. Literature values of fragment yields from interaction of GeV protons with silver targets or with AgBr in emulsions.

| Proton Energy (GeV) | Target | Type of Fragment † | Cross Section (mb) | Freq. per Nuclear Interaction †† | Lit. Ref. |
|---|---|---|---|---|---|
| 1.0 | emul. | $^4$He | 340 ± 60 | | a |
| 2.0 | emul. | $^4$He | 960 ± 130 | | a |
| 3.0 | emul. | $^4$He | 1160 ± 130 | | a |
| 1.0 | Ag | $^6$He | 4 | | b |
| 1.9 | Ag | $^6$He | 7 | | b |
| 2.85 | Ag | $^6$He | 12 | | b |
| 0.93 | emul. | Li | 135 ± 81 | | c |
| 6.2 | emul. | Li($N_H > 8$) | | 0.25 | d |
| 0.95 | emul. | $^8$Li | 1.1 ± 0.8 | | e |
| 1.0 | emul. | $^8$Li | 0.6 ± 0.2 | | a |
| 2.0 | emul. | $^8$Li | 6 ± 1 | | a |
| 2.0 | Ag | $^8$Li | 2.8 ± 1.0 | | f |
| 2.0 | emul. | $^8$Li | 3.0 ± 0.9 | | g |
| 3.0 | emul. | $^8$Li | 4 ± 1 | | a |
| 3.0 | emul. | $^8$Li | 3.4 ± 0.6 | | g |
| 5.7 | emul. | $^8$Li($7 \leq N_H \leq 17$) | | 0.0039 | i |
| 5.7 | | $^8$Li($N_H \geq 17$) | | 0.068 | i |
| 5.7 | emul. | $^8$Li($N_H > 5$) | | 0.013 | e |
| 6.0 | emul. | $^8$Li | 5.1 ± 1.2 | | g |

(continued)

Table I. (Continued)

| Proton Energy (GeV) | Target | Type of Fragment † | Cross Section (mb) | Freq. per Nuclear Interaction †† | Lit. Ref. |
|---|---|---|---|---|---|
| 9. | emul. | $^{8}Li$, $^{8}B$ | 8 | | j |
| 9. | emul. | $^{8}Li(N_H > 8)$ | | 0.02 | k |
| 9. | emul. | $^{8}Li$ | 5.0 ± 1.1 | | g |
| 9. | emul. | $^{8}Li$ | | 0.02 | l |
| 19. | emul. | $^{8}Li$ | | 0.025 | m |
| 24. | emul. | $^{8}Li(N_H > 8)$ | | 0.025 | l |
| 24. | emul. | $^{8}Li$, $^{9}Li$, $^{8}B$ | | 0.0107 | m |
| 25. | emul. | $^{8}Li$, $^{9}Li$, $^{8}B$ | | 0.011 | n |
| 25. | emul. | $^{8}Li$, $^{9}Li$ | 2.0 | | o |
| 28. | emul. | $^{8}Li$ | | 0.014 | p |
| 1.0 | Ag | $^{9}Li$ | 0.22 | | q |
| 2.8 | Ag | $^{9}Li$ | 1.05 | | q |
| 9 | emul. | $^{9}Li$ | | 0.0004 | k |
| 0.66 | emul. | $Z \geq 4$ | 12 | | r |
| 0.93 | emul. | $Z \geq 4$ | 62 ± 11 | | c |
| 9. | emul. | $Z \geq 4$ | 100 | | j |
| 2.0 | emul. | Be(except $^{8}Be$) | 23.3 ± 9.1 | | g |
| 3.0 | emul. | Be(except $^{8}Be$) | 19.6 ± 4.6 | | g |
| 6. | emul. | Be(except $^{8}Be$) | 29.8 ± 9.8 | | g |
| 6.2 | emul. | Be | | 0.09 | d |
| 9. | emul. | Be(except $^{8}Be$) | 26.1 ± 3.6 | | g |

(continued)

Table I. (Continued)

| Proton Energy (GeV) | Target | Type of Fragment † | Cross Section (mb) | Freq. per Nuclear Interaction †† | Lit. Ref. |
|---|---|---|---|---|---|
| 1.0 | Ag | $^{7}$Be | 2.5 | | s |
| 2.2 | Ag | $^{7}$Be | 11.3 | | t |
| 3.0 | Ag | $^{7}$Be | 7.4 | | s |
| 3.0 | Ag | $^{7}$Be | 12.1 | | s |
| 30. | Ag | $^{7}$Be | 18.2 | | t |
| 2. | emul. | $^{8}$Be | 8.2 ± 1.7 | | g |
| 3. | emul. | $^{8}$Be | 7.7 ± 1.3 | | g |
| 6. | emul. | $^{8}$Be | 8.0 ± 1.8 | | g |
| 9. | emul. | $^{8}$Be | 10.4 ± 2.2 | | g |
| 2. | emul. | B | 5.5 ± 1.9 | | g |
| 3. | emul. | B | 8.3 ± 2.7 | | g |
| 6. | emul. | B | 8.5 ± 3.4 | | g |
| 6.2 | emul. | B | | 0.08 | d |
| 9. | emul. | B | 9.0 ± 1.5 | | g |
| 9. | emul. | $^{8}$B($N_H$ > 8) | | 0.0006 | k |
| 24. | emul. | $^{8}$B($N_H$ > 8) | | 0.0014 | l |
| 2.0 | Ag | C | 2.0 ± 0.9 | | g |
| 3. | emul. | C | 2.2 ± 1.3 | | g |

(continued)

Table I. (Continued)

| Proton Energy (GeV) | Target | Type of Fragment† | Cross Section (mb) | Freq. per Nuclear Interaction†† | Lit. Ref. |
|---|---|---|---|---|---|
| 6. | emul. | C | 2.7 ± 1.8 | | g |
| 9. | emul. | C | 2.6 ± 0.8 | | g |
| 3. | Ag | $^{11}C$ | 2.3 | | u |
| 1.0 | Ag | $^{16}C$ | 0.028 | | q |
| 2.8 | Ag | $^{16}C$ | 0.18 | | q |
| 1.0 | Ag | $^{17}N$ | 0.163 | | q |
| 2.8 | Ag | $^{17}N$ | 0.99 | | q |
| 1.0 | Ag | $^{18}F$ | 0.20 | | v |
| 2.0 | Ag | $^{18}F$ | 0.55 | | v |
| 3.0 | Ag | $^{18}F$ | 1.7 | | v |
| 4.5 | Ag | $^{18}F$ | 1.9 | | v |
| 5.9 | Ag | $^{18}F$ | 1.5 | | v |
| 3. | Ag | $^{20}Ne$ | 6.5 | | w |
| 29. | Ag | $^{20}Ne$ | 15 | | w |
| 3. | Ag | $^{21}Ne$ | 6.5 | | w |
| 29. | Ag | $^{21}Ne$ | 15 | | w |
| 3. | Ag | $^{22}Ne$ | 6.1 | | w |
| 29. | Ag | $^{22}Ne$ | 13.7 | | |
| 1. | Ag | $^{24}Ne$ | 0.02 | | t |
| 2. | Ag | $^{24}Ne$ | 0.09 | | t |
| 3. | Ag | $^{24}Ne$ | 0.21 | | t |

(continued)

Table I. (Continued)

| Proton Energy (GeV) | Target | Type of Fragment† | Cross Section (mb) | Freq. per Nuclear Interaction†† | Lit. Ref. |
|---|---|---|---|---|---|
| 3. | Ag | $^{22}$Na | 1.1 | | t |
| 3. | Ag | $^{22}$Na | 1.14 | | h |
| 30. | Ag | $^{22}$Na | 2.2 | | t |
| 1.0 | Ag | $^{24}$Na | 0.30 | | v |
| 2.0 | Ag | $^{24}$Na | 1.4 | | v |
| 3.0 | Ag | $^{24}$Na | 2.7 | | v |
| 3.0 | Ag | $^{24}$Na | 2.1 | | t |
| 3.0 | Ag | $^{24}$Na | 2.24 | | h |
| 4.5 | Ag | $^{24}$Na | 4.1 | | v |
| 5.9 | Ag | $^{24}$Na | 3.3 | | v |
| 30. | Ag | $^{24}$Na | 4.1 | | h |
| 30. | Ag | $^{24}$Na | 4.7 | | t |

†The symbol $N_H$ in this column refers to the total of gray and black tracks accompanying the fragment as observed in the emulsion studies.

††The total cross section for nuclear interaction on Ag by GeV-energy protons is approximately 1200 mb.

[a]Ref. 24. [e]Ref. 10. [i]O. Skjeggestad Thesis, Oslo (1965).

[b]Ref. 62. [f]Ref. 16. [j]Ref. 26.

[c]Ref. 20. [g]Ref. 21. [k]Ref. 28.

[d]Ref. 19. [h]Ref. 56. [l]Ref. 29.

(continued)

Table I. (Continued)

[m] Ref. 31.

[n] Ref. 32.

[o] Ref. 33.

[p] Ref. 34.

[q] Ref. 61.

[r] Ref. 23.

[s] Ref. 58.

[t] Ref. 60.

[u] R. Sharp (unpublished data).

[v] Ref. 59.

[w] Ref. 54.

Table II. Selected literature values of parameters describing fragment energy spectra from emulsions bombarded with high-energy protons.

| Fragment | Proton Energy (GeV) | Most Probable Energy, $E_p$ (MeV) | Temp, $\tau$ (MeV) | Effective Barrier B (MeV) | Velocity v/c | Forward / Backward | Ref. |
|---|---|---|---|---|---|---|---|
| $^{8}Li$ | 9 | ~ 18 | 12 | 3-5 | 0.013 | 1.44 | a |
| $^{8}Li$ | 9 | ~ 15 | 9 | 5 | 0.017 | | b |
| $^{8}Li$ | 9 | | 10 | 5 | 0.015 | 1.7 | c |
| $^{8}Li$ | 19 | | 10 | 5 | 0.015 | 1.65 | d |
| $^{8}Li$ | 24 | ~ 18 | 12 | 3-5 | 0.015 | 1.54 | a |
| $^{8}Li$ | 25 | 18 | 10 | 4 | 0.008 | 1.2 | e |
| $^{8}Li$ | 28 | 20 | 10 | 10 | 0.014 | | f |
| $^{6}Li$ | 25 | 20 | 16 | 4 | 0.007 | 1.2 | e |
| $^{7}Li$ | 25 | 23 | 16 | 4 | 0.007 | 1.2 | e |
| $^{7}Be$ | 25 | 37 | 17 | 15 | 0.0225 | 1.8 | e |
| $^{8}Be$ | 25 | 23 | 11 | 9 | 0.008 | 1.2 | e |
| $^{9}Be$ | 25 | 43 | 17 | 15 | 0.020 | 1.8 | e |
| $^{8}B$ | 25 | ~ 40 | 14 | 18 | 0.020 | 2.0 | e |
| $^{10}B$ | 25 | 47 | 15 | 25 | 0.021 | 1.8 | e |
| $^{10}C$ | 25 | 45 | 14 | 26 | 0.018 | 1.8 | e |
| $^{12}C$ | 25 | 45 | 14 | 26 | 0.018 | 1.8 | e |
| $^{12}N$ | 25 | 60 | 14 | 37 | 0.019 | 1 | e |
| $^{14}N$ | 25 | 65 | 14 | 37 | 0.018 | 1 | e |

(continued)

Table II (continued)

[a]Reference 22.

[b]Reference 30.

[c]Reference 27.

[d]Reference 31.

[e]Reference 35.

[f]Reference 34.

Table III. Fragment energy parameters from emulsions exposed to cosmic rays, $\pi$ and K mesons, and antiprotons.

| Type of Bombarding Particle | Fragment | Most Probable Energy, $E_p$ (MeV) | Temp, $\tau$ (MeV) | Effective Barrier B (MeV) | Velocity v/c | Forward / Backward | Ref. |
|---|---|---|---|---|---|---|---|
| cosmic rays | $^{8}$Li($N_H$ = 7-35) | 18-20 | 11.5 | 6 | 0.016 | 1.5 | a |
| cosmic rays | $^{8}$Li | | 9.5 | 5 | | | b |
| cosmic rays | $^{8}$Be | 44 | 19 | 25 | | | b |
| 4.5 GeV $\pi^-$ | $^{8}$Li | | 11 | 8 | | | b |
| 4.5 GeV $\pi^-$ | $^{8}$Li | 17 | 11 | 6 | 0.018 | 1.7 | c |
| | Be | | 15 | 6 | | 2.8 | c |
| 17.2 GeV $\pi^-$ | $^{8}$Li | | 8 | 7 | 0.010 | 2.0 | d |
| | $^{8}$Be | | 8 | 9 | 0.01 | | d |
| 1.5 GeV $K^-$ | $^{8}$Li | | 7 | 10 | 0.01 | 1.7 | e |
| 3 GeV $K^-$ | $^{8}$Li | ~ 18 | 7 | 9 | 0.01 | 1.6 | f |
| 5 GeV anti-p | $^{7}$Li | ~ 18 | 12.2 | 16 | 0.0055 | | g |
| | $^{8}$Li | ~ 13 | 13.9 | 17 | 0.0055 | | g |
| | $^{9}$Be | ~ 27 | 16 | 17.8 | 0.0055 | | g |
| 5 GeV anti-p | $^{8}$Li | 19 | 11.2 | 5.8 | | 0.9 ± 0.1 | h |
| 5 GeV anti-p | $^{8}$Li($N_H$ > 7) | ~ 15 | 13.9 | 17 | 0.0055 | | i |

(continued)

Table III (continued)

[a]Reference 6.

[b]Reference 5.

[c]Reference 40.

[d]Reference 33.

[e]Reference 44.

[f]Reference 51.

[g]Reference 49.

[h]Reference 48.

[i]Reference 46.

Table IV. Counter telescopes used in this study. The numbers given are the thicknesses in microns of the ΔE and E counters, followed in parenthesis by the lower discriminator setting in MeV of the E counter.

| Target | 1.0 mg/cm$^2$ Ag | 7.1 mg/cm$^2$ Ag | 25.9 mg/cm$^2$ Ag |
|---|---|---|---|
| Isotope | | | |
| $^{1-3}$H | | 100-1500(2), 250-3000(4) | 250-5000(5) |
| $^{3}$He, $^{4}$He | 20-168(3) | 61-250(4), 100-1500(2), 250-3000(4) | 250-5000(5) |
| $^{6}$He, $^{6-9}$Li | 20-168(3) | 61-250(4), 168-3000(20) | |
| $^{7}$Be | 20-168(6) | 61-250(10), 168-3000(20) | |
| $^{9,10}$Be, $^{8,10-13}$B | 20-168(6) | 61-250(10) | |
| $^{10-14}$C, $^{14,15}$N | | 61-250(10) | |
| C - Si | 20-168(10) | | |



UCRL-19991

Table V. Total cross sections and forward-to-backward ratios for fragments from silver irradiated by 5.5-GeV protons

| Fragment | σ (mb) | F/B |
|---|---|---|
| $^{1}H$ | 3990[a] | |
| $^{2}H$ | 1240[a] | |
| $^{3}H$ | 690[a] | |
| $^{3}He$ | 345[b] | 1.23 |
| $^{4}He$ | 2030 | 1.16 |
| $^{6}He$ | 19.2 | 1.36 |
| $^{6}Li$ | 55 | 1.30 |
| $^{7}Li$ | 69 | 1.38 |
| $^{8}Li$ | 12.8 | 1.50 |
| $^{9}Li$ | 2.6 | 1.74 |
| $^{7}Be$ | 17.4[c] | 1.42 |
| $^{9}Be$ | 15.4 | 1.39 |
| $^{10}Be$ | 10.1 | 1.38 |

[a]Hydrogen yields refer only to that part of the spectrum lying below 28, 32, and 42 MeV for the isotopes $^{1}H$, $^{2}H$, and $^{3}H$, respectively.

[b]In the $^{3}He$ case a correction of 8.8% was applied for the unmeasured part of the spectrum lying above 90 MeV.

[c]Absolute value determined by radiochemistry (see appendix of Ref. 1); all other values in this table were normalized to this value.

Table VI. Parameters obtained from curve fitting

| Nuclide | Nominal Coulomb Barrier B (MeV) | $\langle k \rangle \pm \Delta$ | Peak Energy at 90° $E_p$(MeV) | $\tau$ (MeV) | $\tau_{HE}$ (MeV) | Moving System velocity $\langle v \rangle /c$ |
|---|---|---|---|---|---|---|
| $^{3}He$ | 13.7 | 0.39 | 14 | 8 | 13 | < 0.003 |
| $^{4}He$ | 13.4 | 0.55 | 13 | 6 | 13 | < 0.003 |
| $^{6}He$ | 13.0 | | ≈ 13 | | | |
| $^{6}Li$ | 19. | 0.45 ± 0.1 | 17 | 11 | 19 | 0.008 ± 0.002 |
| $^{7}Li$ | 19. | 0.45 ± 0.1 | 18 | 11 | 23 | 0.008 ± 0.002 |
| $^{8}Li$ | 18. | | 18 | 11 | | 0.008 |
| $^{7}Be$ | 24. | 0.5 ± 0.2 | 22 | 11 | 21 | 0.008 ± 0.003 |
| $^{9}Be$ | 24. | ≈ 0.45 | ≈ 20 | 10 | 13 | |
| $^{10}Be$ | 24. | 0.45 | ≈ 21 | 11 | 13 | 0.006 ± 0.002 |
| $^{8}B$ | 29. | | < 24 | 13 | 15 | |
| $^{10}B$ | 29. | | < 26 | 11 | 15 | |
| $^{11}B$ | 29. | | < 26 | 11 | 15 | |
| $^{12}B$ | 28. | | < 32 | 11 | 13 | |
| $^{13}B$ | 28. | | < 30 | 11 | 13 | |
| C | 33.3 | | < 33 | | 17 | |
| N | 37. | | < 38 | | 13 | |
| O | 41. | | < 43 | | 12 | |
| F | | | < 50 | | 13 | |
| Ne | | | < 52 | | 13 | |
| Na | | | < 56 | | 13 | |
| Mg | | | < 64 | | 14 | |
| Al | | | < 68 | | 13 | |
| Si | | | < 70 | | 9 | |

Table VII. Comparison of fragment energy characteristics (This work and Stein)

| Nuclide | $E_p$ Most Prob. Energy (MeV) | Temp $\tau$ (MeV) | Effective Barrier (MeV) | Velocity v/c | Forward / Backward | Ref. P=Present work S=Stein |
|---|---|---|---|---|---|---|
| $^{6}Li$ | 17 | 11 | 8.5 | 0.008 | 1.3 | P |
| $^{6}Li$ | 20 | 16 | 4 | 0.007 | 1.2 | S |
| $^{7}Li$ | 18 | 11 | 8.5 | 0.008 | 1.38 | P |
| $^{7}Li$ | 23 | 16 | 4 | 0.007 | 1.2 | S |
| $^{8}Li$ | 18 | 11 | 9 | 0.008 | 1.50 | P |
| $^{8}Li$ | 18 | 10 | 4 | 0.008 | 1.2 | S |
| $^{7}Be$ | 22 | 11 | 11 | 0.008 | 1.42 | P |
| $^{7}Be$ | 37 | 17 | 15 | 0.022 | 1.8 | S |
| $^{8}Be$ | (undetected) | | | | | P |
| $^{8}Be$ | 23 | 11 | 9 | 0.008 | 1.2 | S |
| $^{9}Be$ | ~ 20 | 10 | 11 | —— | 1.39 | P |
| $^{9}Be$ | 43 | 17 | 15 | 0.020 | 1.8 | S |
| $^{10}Be$ | 21 | 11 | 11 | 0.006 | 1.38 | P |
| $^{10}Be$ | — | — | | —— | —— | S |
| $^{8}B$ | < 24 | 13 | | —— | | P |
| $^{8}B$ | ~ 40 | 14 | 18 | 0.020 | 2.0 | S |

(continued)

Table VII (continued)

| Nuclide | $E_p$ Most Prob. Energy (MeV) | Temp $\tau$ (MeV) | Effective Barrier (MeV) | Velocity v/c | Forward / Backward | Ref. P=Present work S=Stein |
|---|---|---|---|---|---|---|
| $^{10}B$ | < 26 | 11 | | ——— | | P |
| $^{10}B$ | 47 | 15 | 25 | 0.021 | 1.8 | S |
| $C_{(all\ isotopes)}$ | < 33 | 17 | | | | P |
| $^{14}C$ | 45 | 14 | 26 | 0.018 | 1.8 | S |
| $N_{(all\ isotopes)}$ | < 38 | 13 | | ——— | | P |
| $^{14}N$ | 65 | 14 | 37 | .018 | 1 | S |

## FIGURE CAPTIONS

Fig. 1. Simplified schematic diagram of the particle identification system with a single ΔE counter.

Fig. 2. Representative particle spectra for fragments from silver as measured by a telescope with a 61-μm ΔE detector and 250-μm E detector except for part (a) which was measured with a 100-μm, 1500-μm ΔE-E detector telescope.

Fig. 3. Spectrum of elements ejected from a 1.0 mg/cm$^2$ silver target and measured in a telescope with a 20-μm ΔE detector.

Fig. 4. Energy spectra for the isotopes $^4$He, $^6$Li, and $^7$Be ejected from silver targets at 90° to the beam. For each isotope, data points from three measurements with different telescopes are shown.

Fig. 5. Energy spectra for hydrogen isotopes at 5 angles to the beam. Solid lines were drawn through the data points. Dashed line shows extrapolation to zero energy.

Fig. 6. Energy spectra for helium isotopes at 5 angles to the beam. Solid lines were drawn through the data points. Dashed line shows extrapolation to zero energy.

Fig. 7. Energy spectra for lithium isotopes at 5 angles to the beam. Spectra for 20°, 45°, 90°, 135°, and 160° appear in order with the 20° spectrum lying highest. Solid lines were drawn through the data points. Dashed lines show extrapolation to zero energy.

Fig. 8. Energy spectra for beryllium isotopes at 5 angles to the beam. See caption for Fig. 7.

Fig. 9. Semilogarithmic energy spectra for boron isotopes at 5 angles to the beam. Spectra for 20°, 45°, 90°, 135°, and 160° appear in order with the 20° spectrum lying highest.

Fig. 10. Energy spectra for carbon isotopes at 5 angles to the beam. See caption for Fig. 9.

Fig. 11. Energy spectra for nitrogen isotopes at 5 angles to the beam. See caption for Fig. 9.

Fig. 12. Composite figure showing energy spectra of isotopes of H through N at 90° to the beam. Curves are displaced by the scale factors listed at the upper right of the figure.

Fig. 13. High energy portion of energy spectra for the elements C through Si measured at 3 angles to the beam with a telescope containing a 20-μm ΔE detector.

Fig. 14. Laboratory angular distributions of isotopes of H, He, Li, and Be obtained by integration of curves from Figs. 5-8.

Fig. 15. Experimental data for $^{7}$Li at 20°, 90°, and 160° compared with theoretical curves with the following parameter choices: $\tau = 11$, $\langle k \rangle = 0.5$, $v/c = 0.008$, $n = 2$, $\Delta = 0.1$. The curves were normalized to the data at the peak of the 90° data. Scales are displaced for the 20° and 160° curves.

Fig. 16. Experimental data for $^{7}$Be at 20°, 90°, and 160° compared with theoretical curves with the following parameter choices: $\tau = 11$, $\langle k \rangle = 0.5$, $v/c = 0.008$, $n = 2$, $\Delta = 0.1$. The curves were normalized to the data at the peak of the 90° data. Scales are displaced for the 20° and 160° curves.

Fig. 17. Experimental data for the element carbon at 20°, 90°, and 160° compared with theoretical curves based on the following parameters: $\tau = 11$, $\langle k \rangle = 0.5$, $v/c = 0.006$, $N = 1.0$, and $\Delta = 0.1$. The curves were normalized to the data for 90° only, which are represented by solid dots.

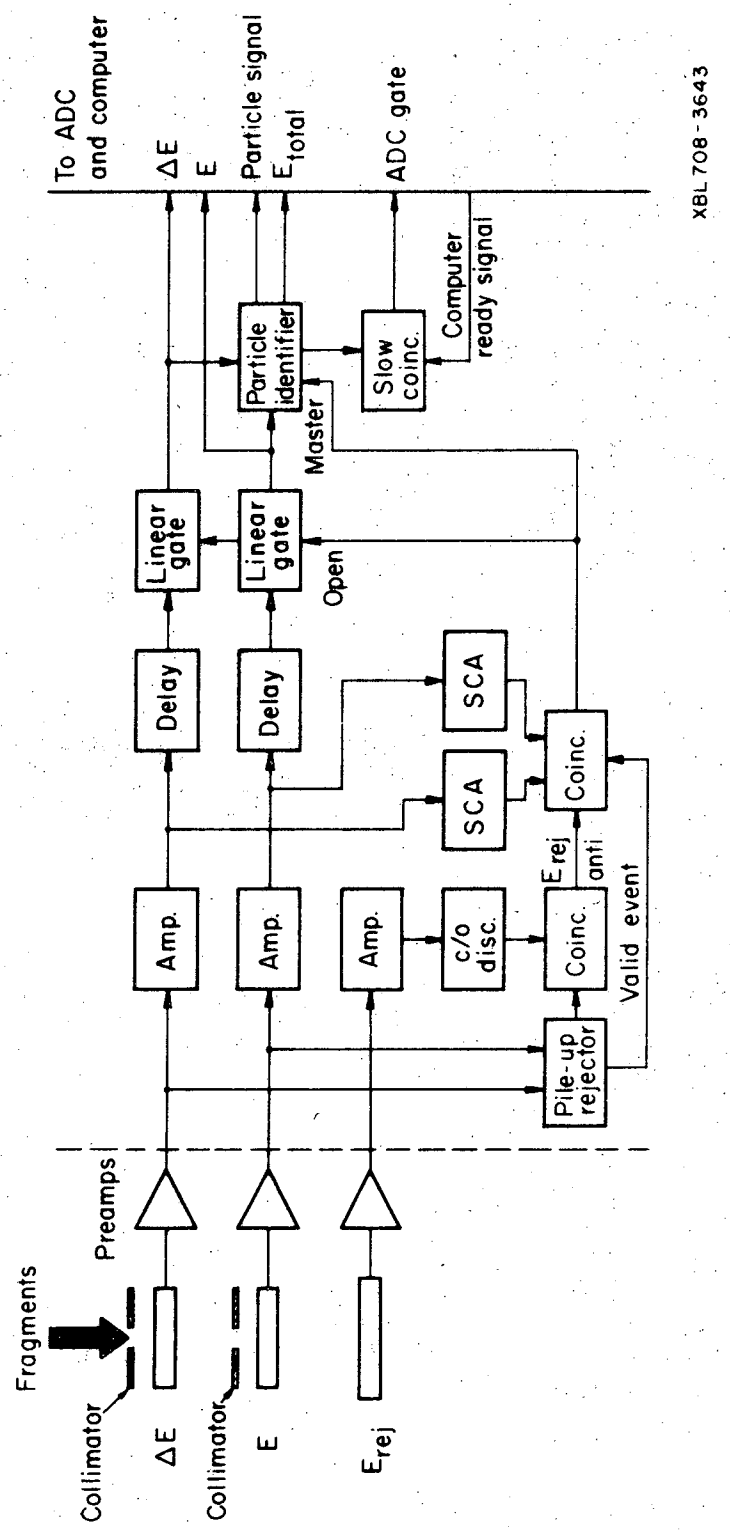
To ADC and computer
ΔE
E
Particle signal
E total
ADC gate
XBL 708-3643
Particle identifier
Slow coinc.
Computer ready signal
Master
Linear gate
Linear gate
Open
Delay
Delay
SCA
SCA
Coinc.
Amp.
Amp.
Amp.
c/o disc.
Coinc.
E rej
anti
Valid event
Pile-up rejector
Preamps
Fragments
Collimator
ΔE
Collimator
E
E rej

Fig. 1

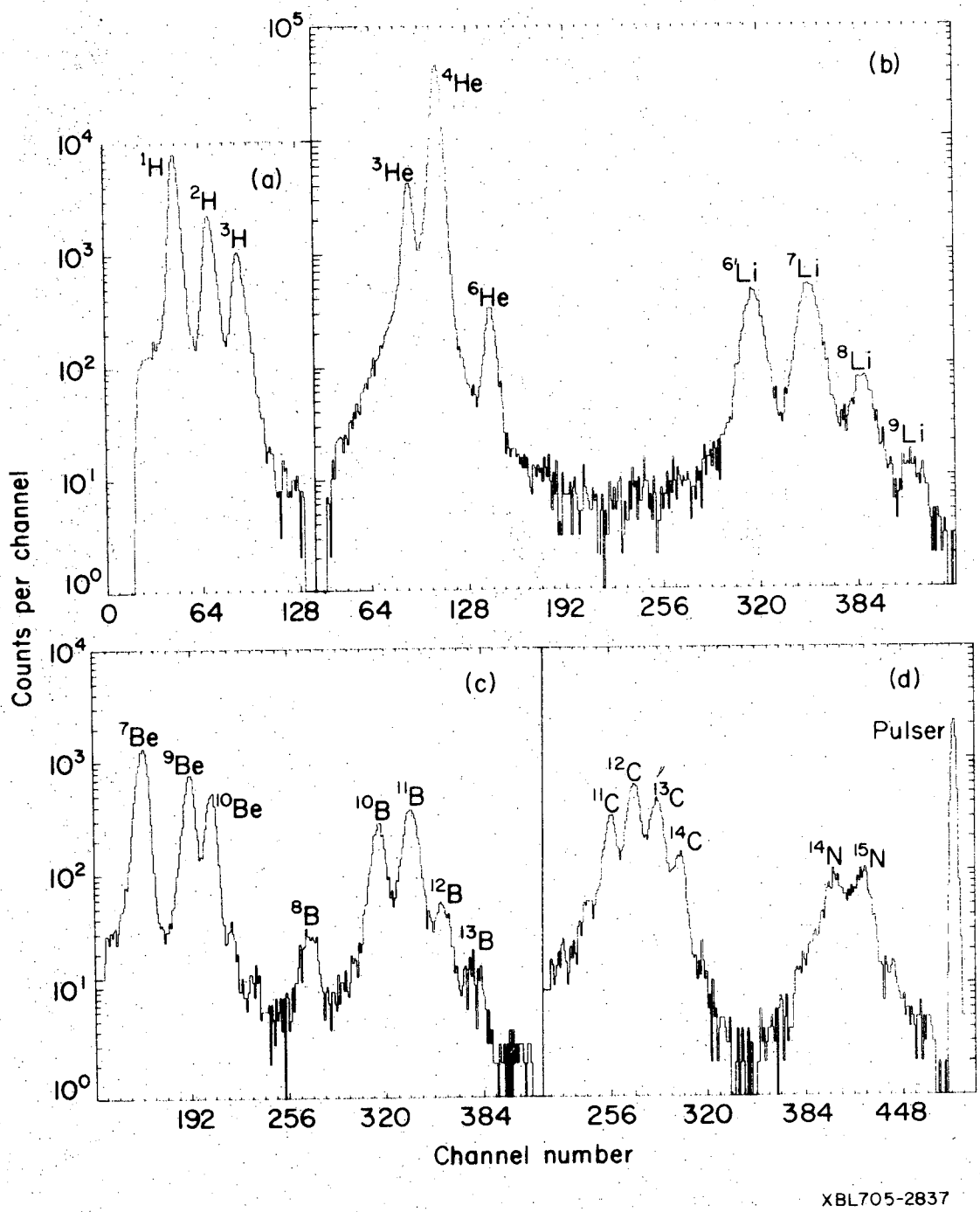
(a)
(b)
(c)
(d)
$^{1}$H
$^{2}$H
$^{3}$H
$^{3}$He
$^{4}$He
$^{6}$He
$^{6}$Li
$^{7}$Li
$^{8}$Li
$^{9}$Li
$^{7}$Be
$^{9}$Be
$^{10}$Be
$^{8}$B
$^{10}$B
$^{11}$B
$^{12}$B
$^{13}$B
$^{11}$C
$^{12}$C
$^{13}$C
$^{14}$C
$^{14}$N
$^{15}$N
Pulser
Counts per channel
Channel number
XBL705-2837

Fig. 2

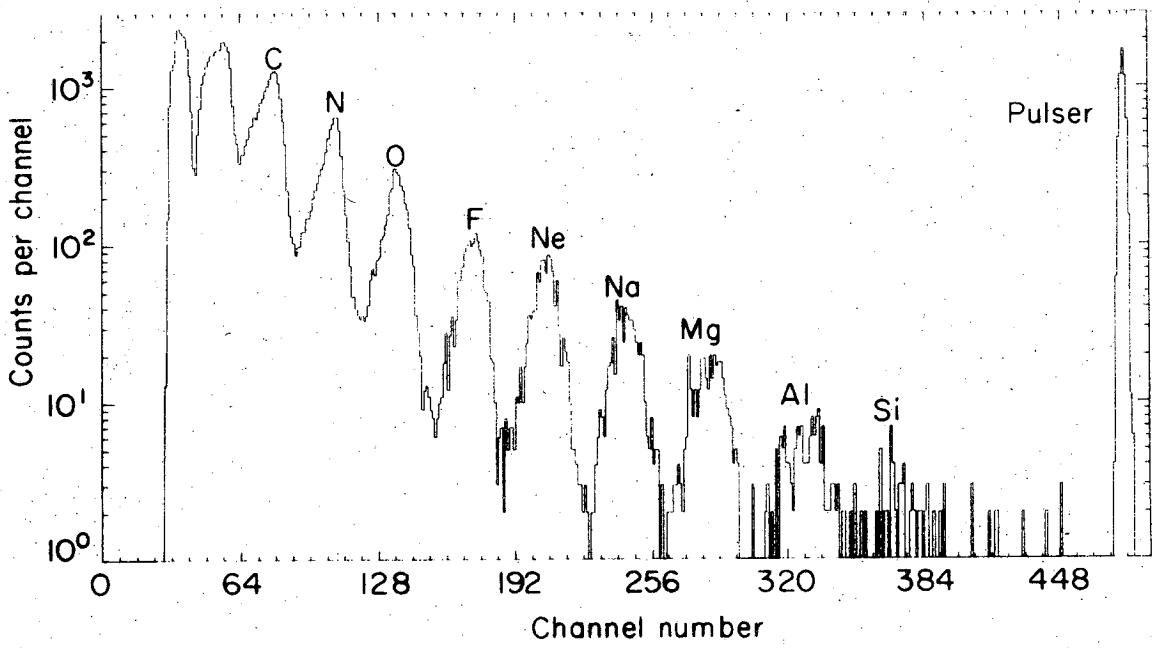


XBL705-2846

Fig. 3

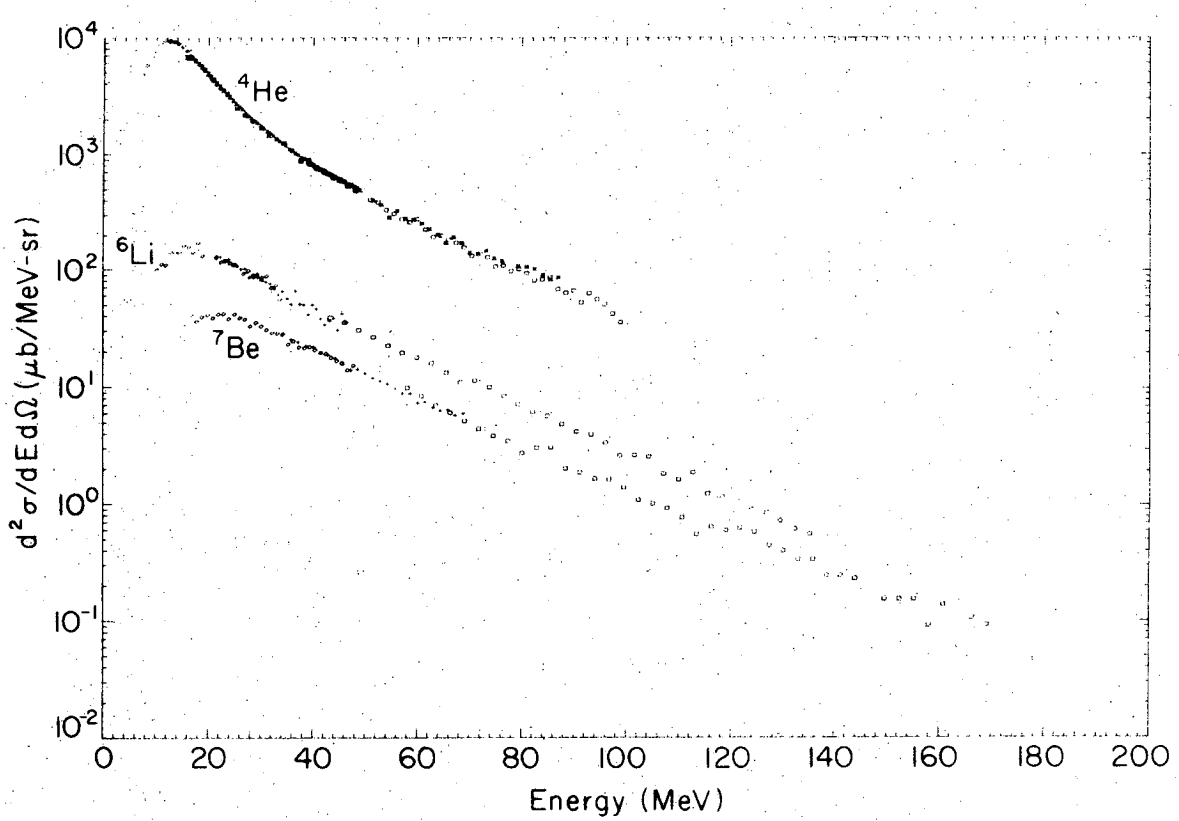


XBL705-2831

Fig. 4

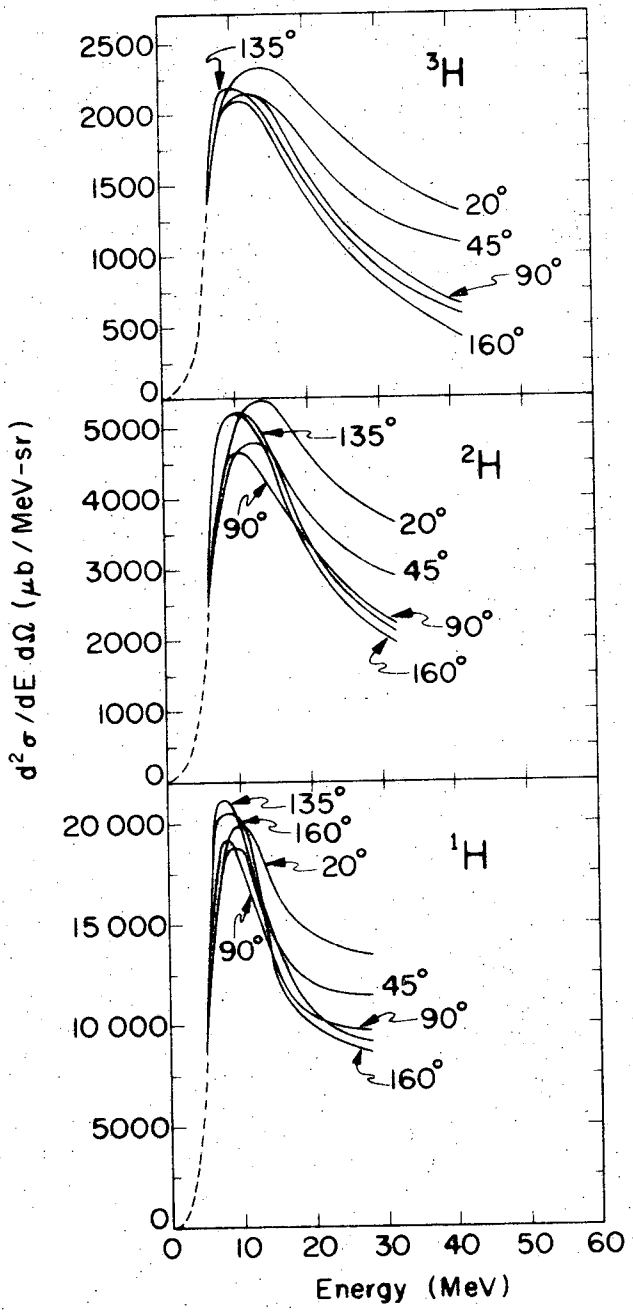


XBL705-2844

Fig. 5

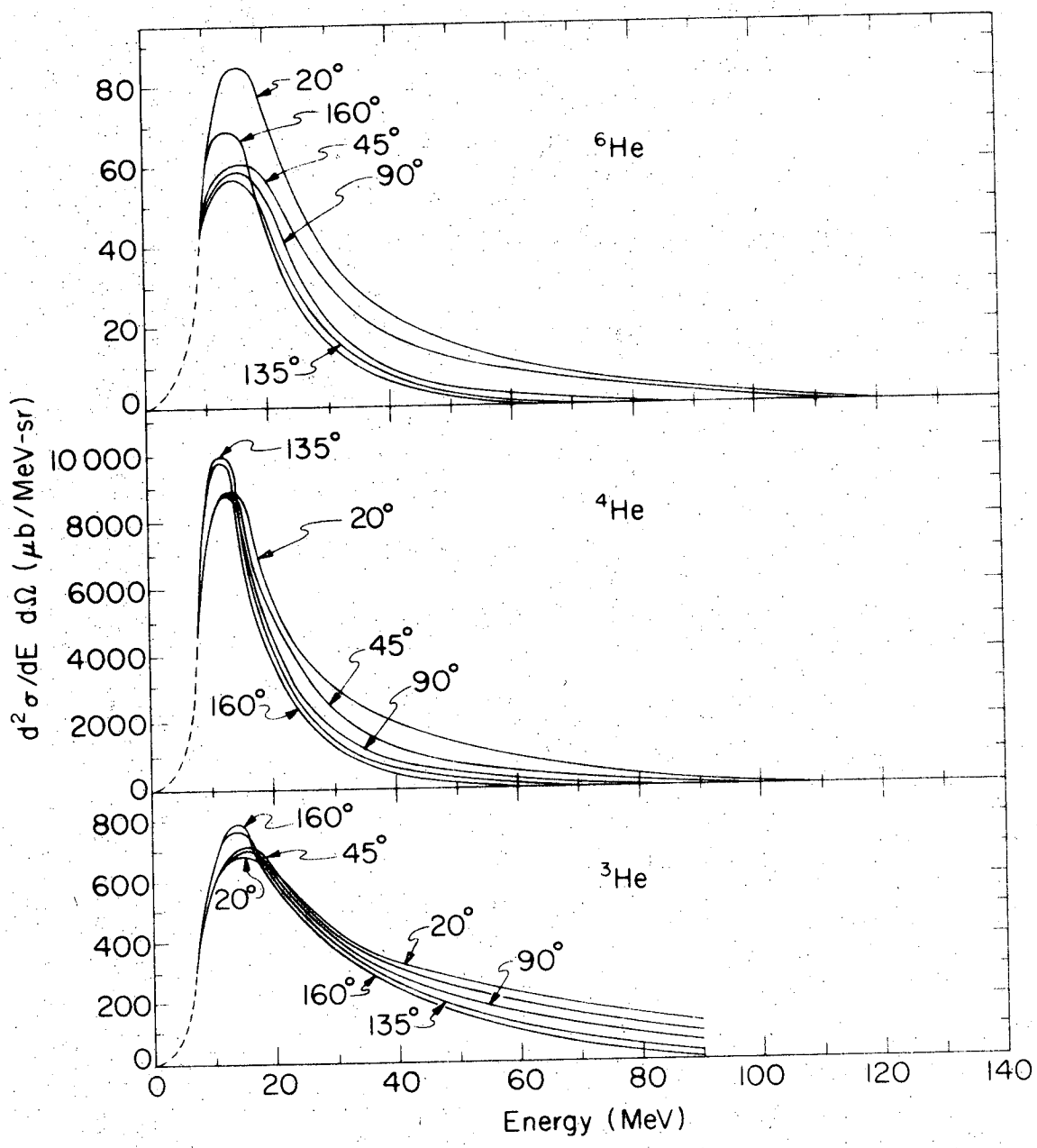


XBL705-2842

Fig. 6

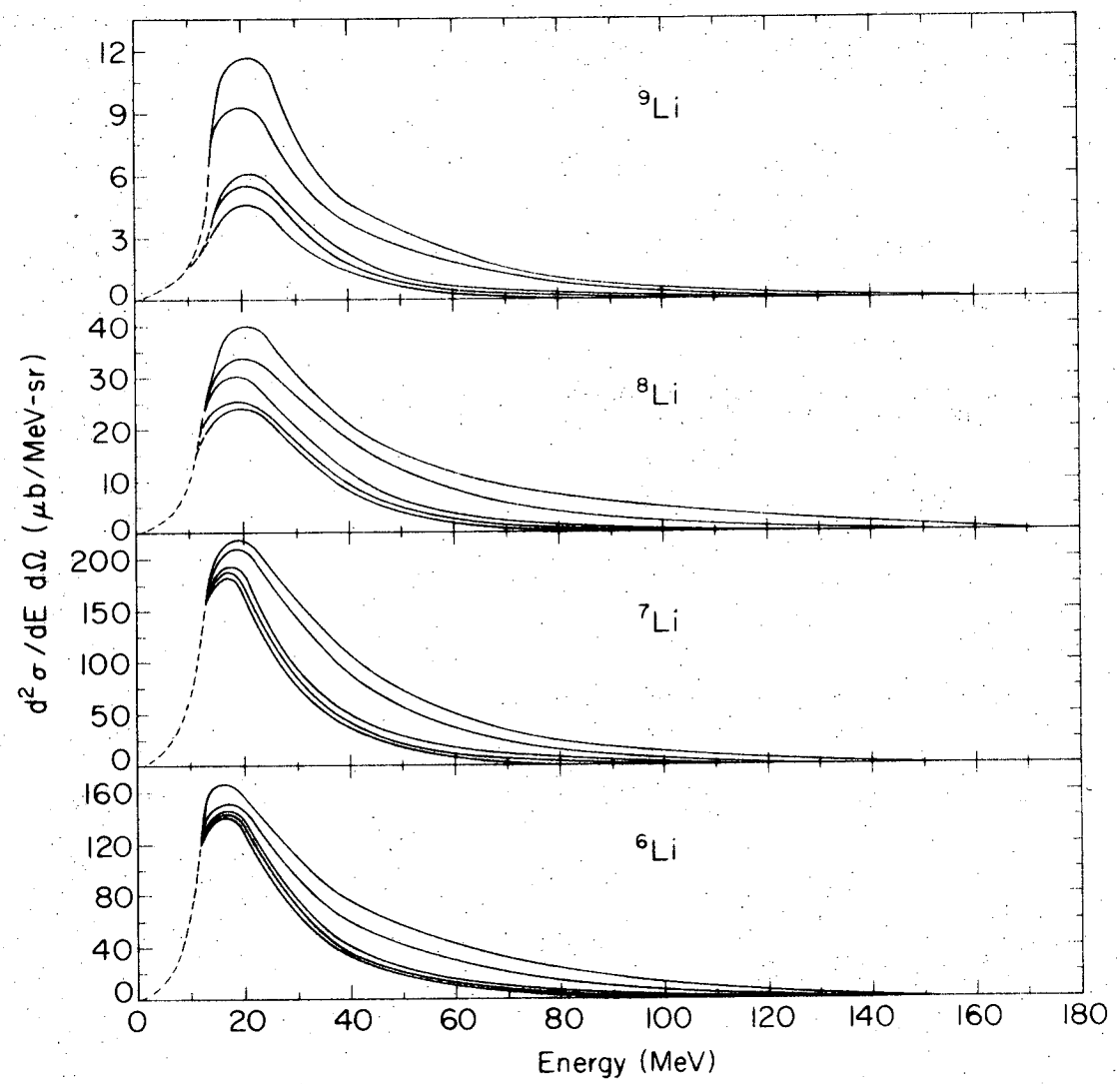
$^9$Li
$^8$Li
$^7$Li
$^6$Li
$d^2\sigma/dE\ d\Omega$ ($\mu$b/MeV-sr)
Energy (MeV)
0
20
40
60
80
100
120
140
160
180
XBL705-2838

Fig. 7

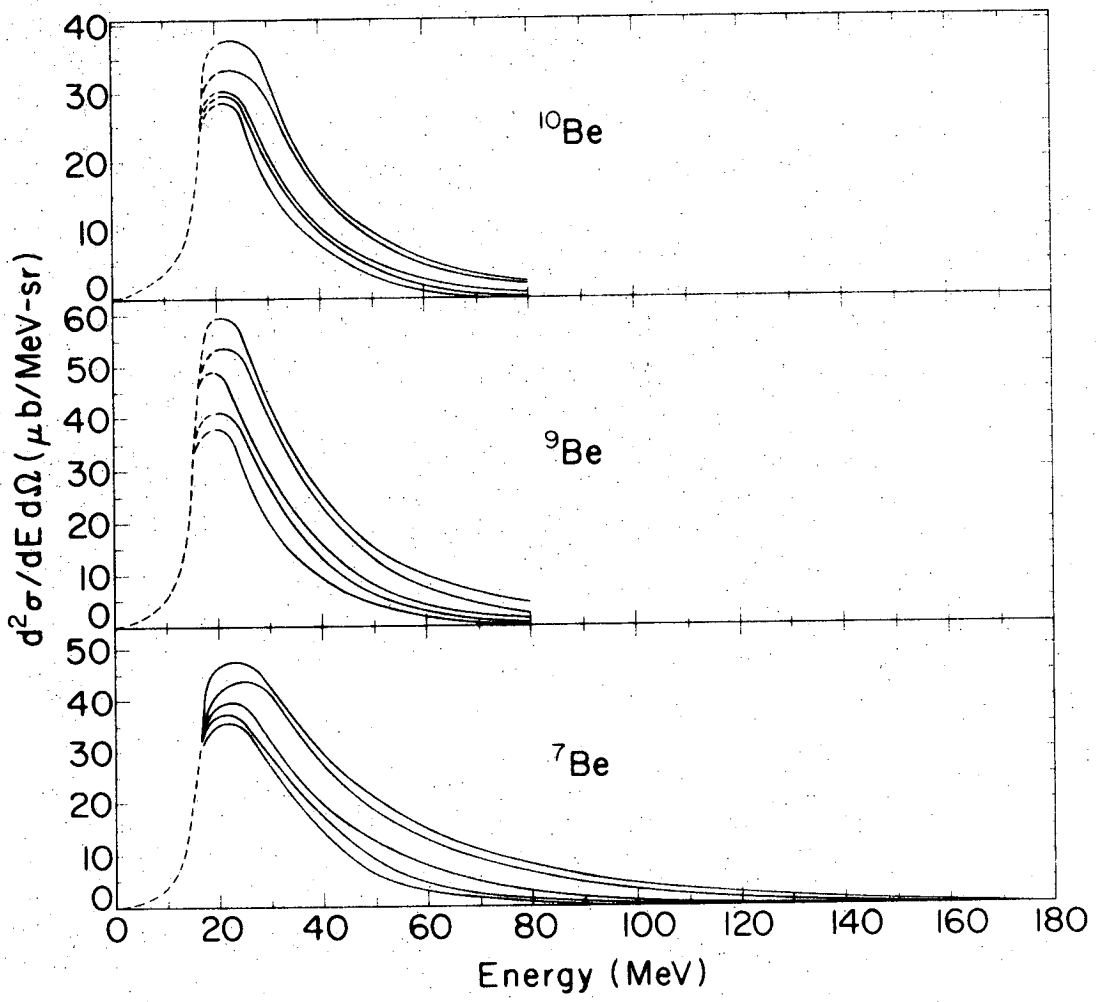


XBL705-2834

Fig. 8

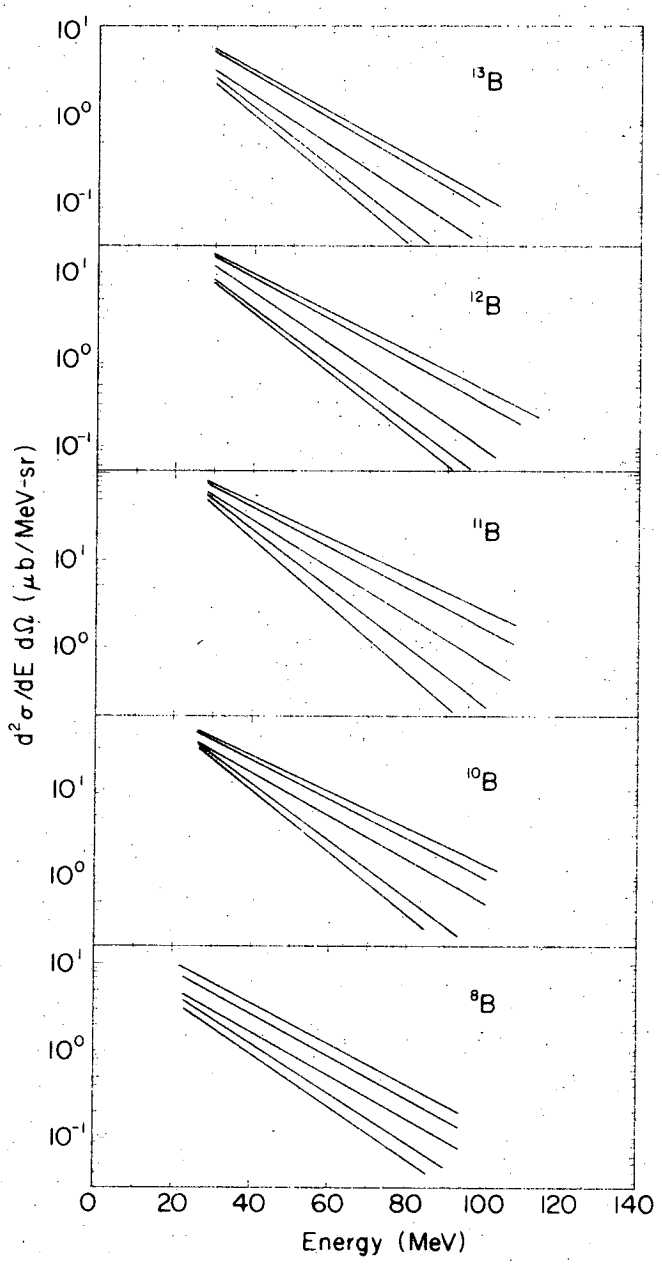
$^{13}$B
$^{12}$B
$^{11}$B
$^{10}$B
$^{8}$B
$d^2\sigma/dE\ d\Omega$ ($\mu$b/MeV-sr)
Energy (MeV)
XBL705-2847

Fig. 9

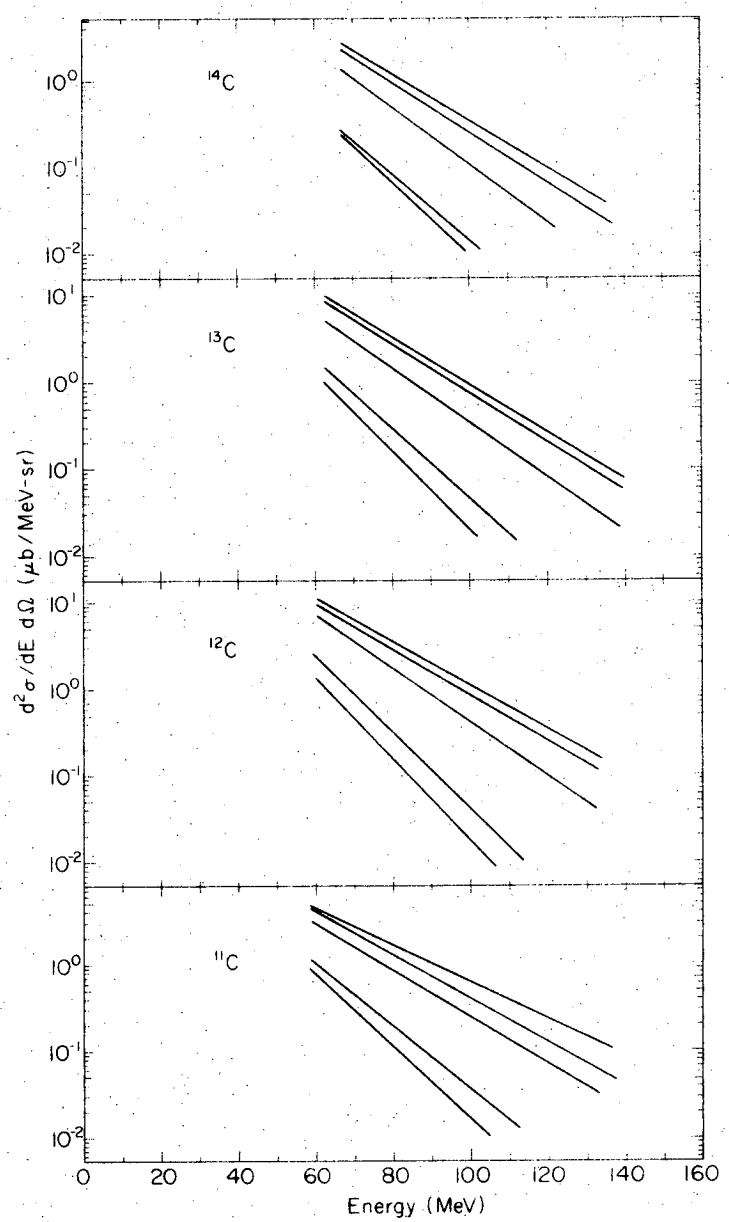
$^{14}C$
$^{13}C$
$^{12}C$
$^{11}C$
$d^2\sigma/dE\ d\Omega$ ($\mu$b/MeV-sr)
Energy (MeV)
0
20
40
60
80
100
120
140
160
$10^0$
$10^{-1}$
$10^{-2}$
$10^1$
XBL705-2841

Fig. 10

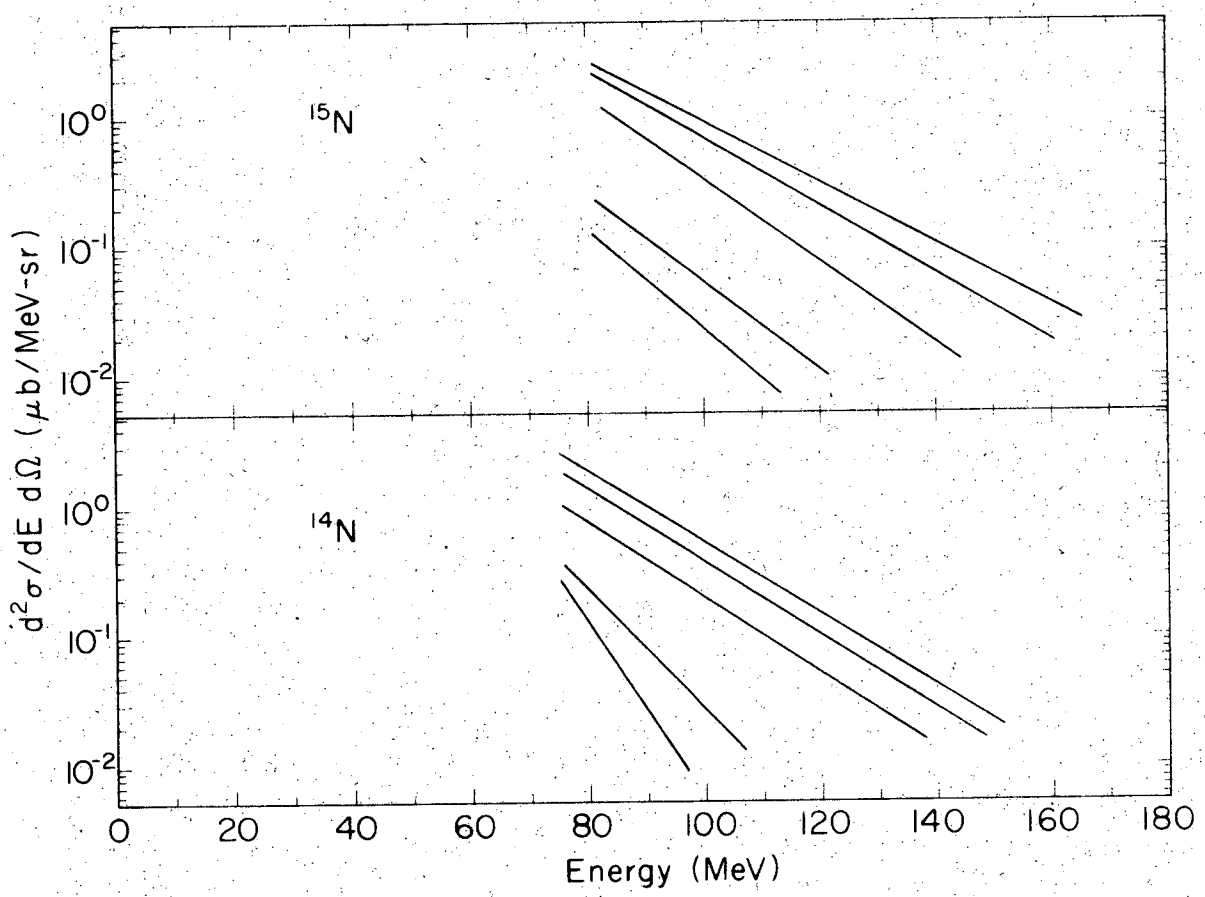


XBL705-2840

Fig. 11

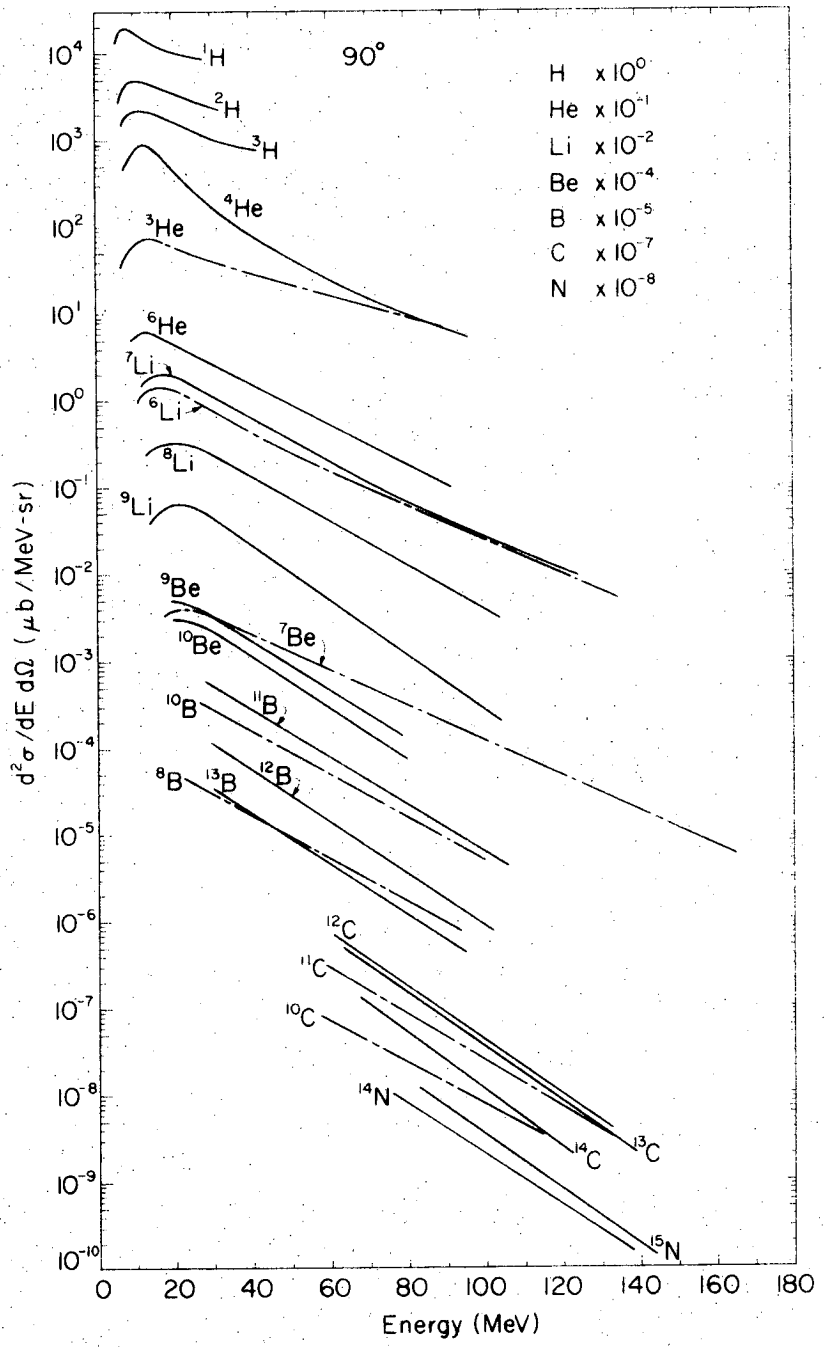
90°
H x 10^0
He x 10^-1
Li x 10^-2
Be x 10^-4
B x 10^-5
C x 10^-7
N x 10^-8
1H
2H
3H
4He
3He
6He
7Li
6Li
8Li
9Li
9Be
7Be
10Be
10B
11B
8B
13B
12B
12C
11C
10C
14N
14C
13C
15N
d²σ/dE dΩ (μb/MeV-sr)
Energy (MeV)
0
20
40
60
80
100
120
140
160
180
XBL705-2845

Fig. 12

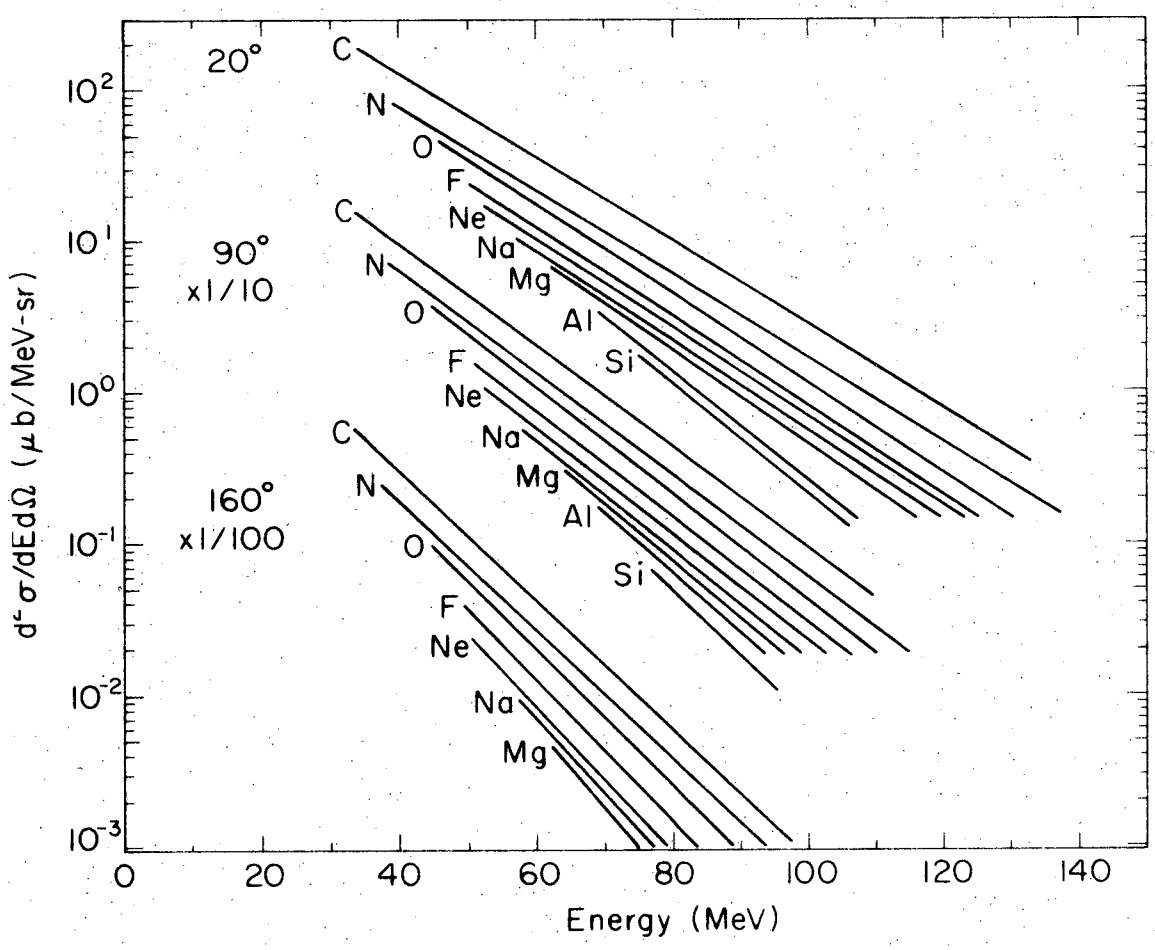


XBL705-2839

Fig. 13

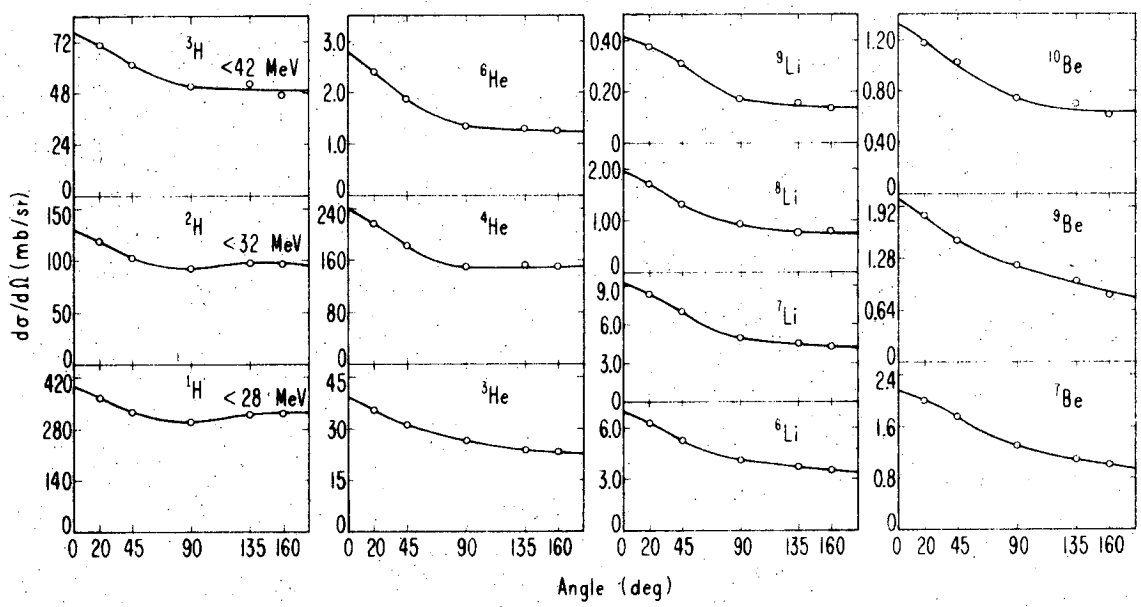
$^{3}$H <42 MeV
$^{2}$H <32 MeV
$^{1}$H <28 MeV
$^{6}$He
$^{4}$He
$^{3}$He
$^{9}$Li
$^{8}$Li
$^{7}$Li
$^{6}$Li
$^{10}$Be
$^{9}$Be
$^{7}$Be
dσ/dΩ (mb/sr)
Angle (deg)
0 20 45 90 135 160
XBL705-2843

Fig. 14

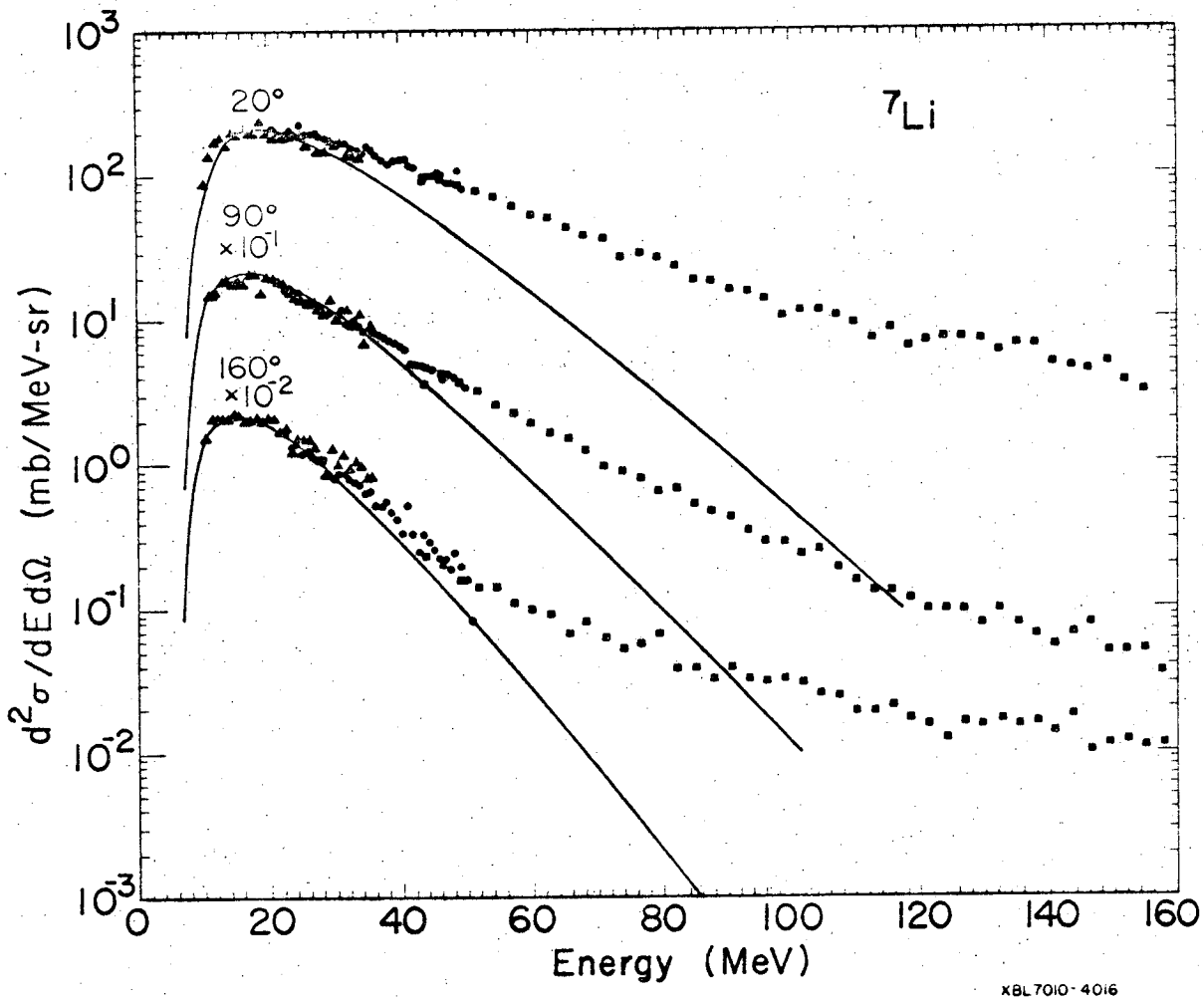
$10^3$
$10^2$
$10^1$
$10^0$
$10^{-1}$
$10^{-2}$
$10^{-3}$
20°
90°
×10⁻¹
160°
×10⁻²
⁷Li
$d^2\sigma/dE\,d\Omega$ (mb/MeV-sr)
0
20
40
60
80
100
120
140
160
Energy (MeV)
XBL7010-4016

Fig. 15

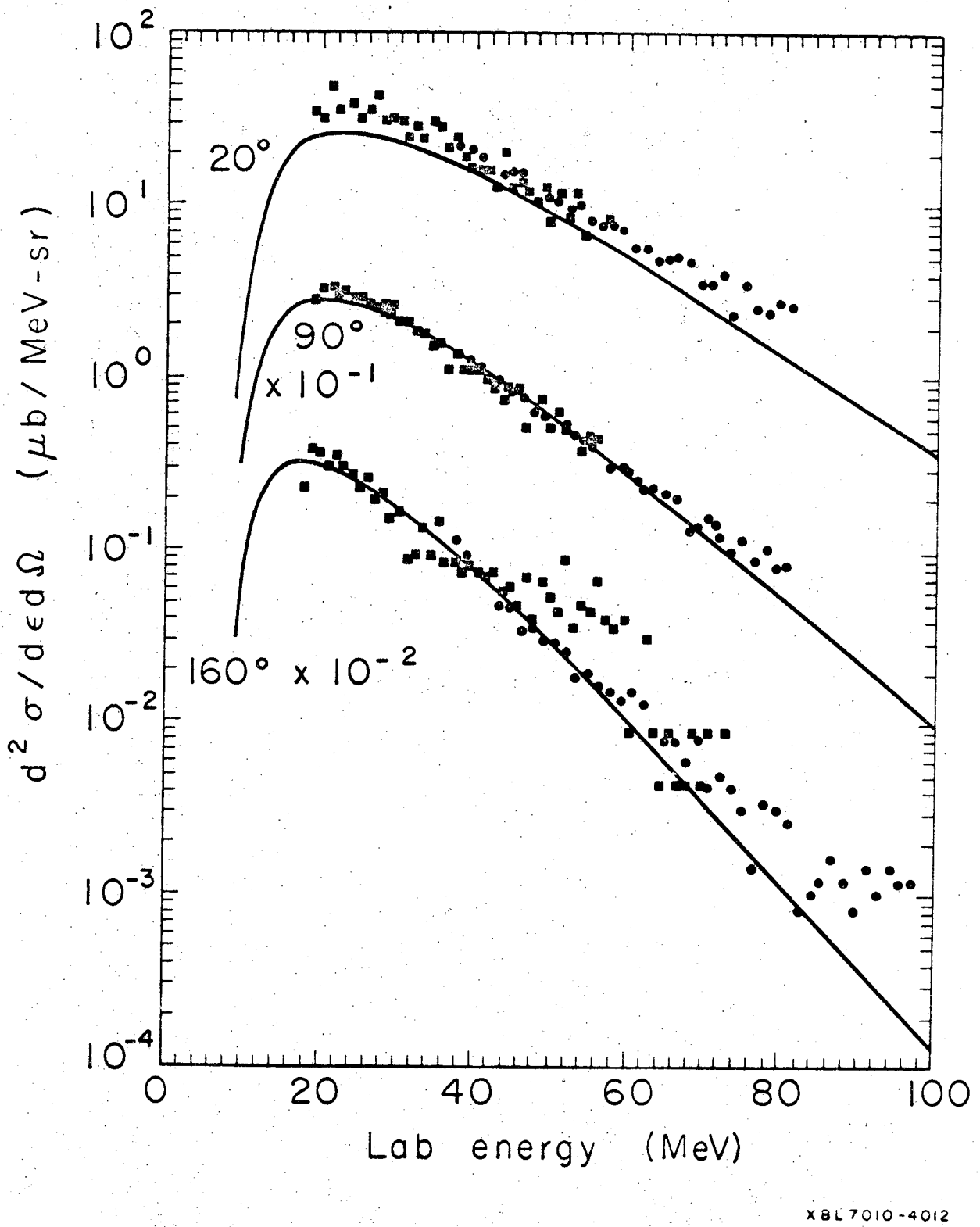
$10^2$
$10^1$
$10^0$
$10^{-1}$
$10^{-2}$
$10^{-3}$
$10^{-4}$
20°
90°
x $10^{-1}$
160° x $10^{-2}$
$d^2\sigma/d\epsilon d\Omega$ ($\mu$b / MeV-sr)
0
20
40
60
80
100
Lab energy (MeV)
XBL7010-4012

Fig. 16

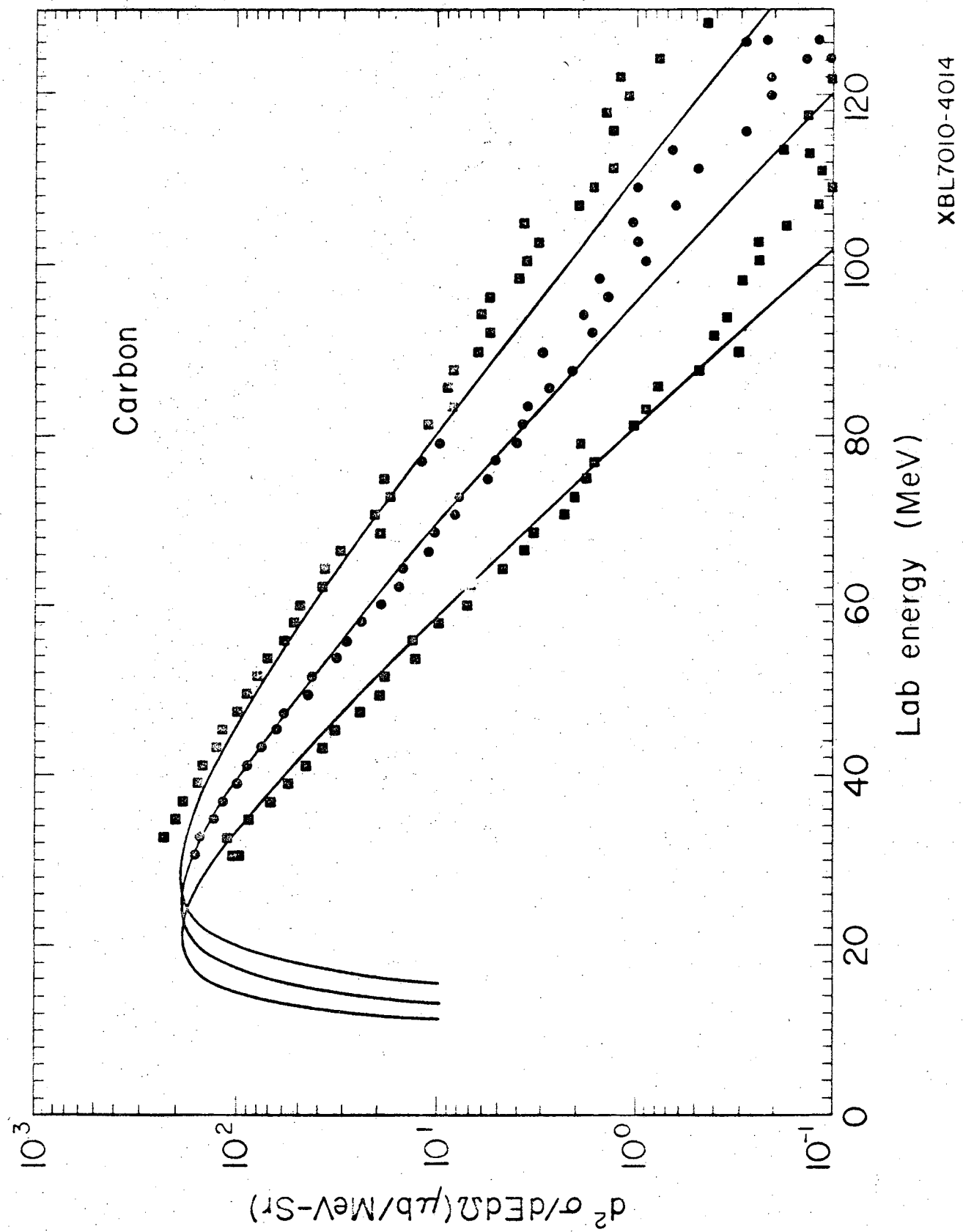
Carbon
$d^2\sigma/dE d\Omega$ ($\mu$b/MeV-Sr)
$10^3$
$10^2$
$10^1$
$10^0$
$10^{-1}$
0
20
40
60
80
100
120
Lab energy (MeV)
XBL7010-4014

Fig. 17

LEGAL NOTICE

*This report was prepared as an account of work sponsored by the United States Government. Neither the United States nor the United States Atomic Energy Commission, nor any of their employees, nor any of their contractors, subcontractors, or their employees, makes any warranty, express or implied, or assumes any legal liability or responsibility for the accuracy, completeness or usefulness of any information, apparatus, product or process disclosed, or represents that its use would not infringe privately owned rights.*

*TECHNICAL INFORMATION DIVISION*
*LAWRENCE RADIATION LABORATORY*
*UNIVERSITY OF CALIFORNIA*
*BERKELEY, CALIFORNIA 94720*